

Statistical characteristics of the observed Ly- α forest and the shape of the initial power spectrum

M. Demiański^{1,2}, A.G. Doroshkevich³, V.I. Turchaninov⁴

¹*Institute of Theoretical Physics, University of Warsaw, 00-681 Warsaw, Poland*

²*Department of Astronomy, Williams College, Williamstown, MA 01267, USA*

³*Astro Space Center of Lebedev Physical Institute of Russian Academy of Sciences, 117997 Moscow, Russia*

⁴*Keldysh Institute of Applied Mathematics Russian Academy of Sciences, 125047 Moscow, Russia*

Accepted ..., Received ..., in original form

ABSTRACT

We analyze basic properties of about 6000 Lyman- α absorbers observed in high resolution spectra of 19 quasars. We compare their observed characteristics with predictions of our model of formation and evolution of absorbers and dark matter (DM) pancakes and voids based on the Zel'dovich theory of gravitational instability. This model asserts that absorbers are formed in the course of both linear and non linear adiabatic and shock compression of DM and gaseous matter. Our model is consistent with simulations of structure formation, describes reasonably well the Large Scale Structure (LSS) observed in the distribution of galaxies at small redshifts and emphasizes the generic similarity of the process of formation of LSS and absorbers. Using this model we are able to link the column density and overdensity of DM and gaseous component with the observed column density of neutral hydrogen, redshifts and Doppler parameters of absorbers. We show that the colder absorbers are associated with rapidly expanded underdense regions of galactic scale.

We extend the method of measuring the power spectrum of initial perturbations proposed in Demiański & Doroshkevich (2003b). The observed separations between absorbers and their DM column density are linked with the correlation function of the initial velocity field. Applying this method to our sample of absorbers we recover the CDM like power spectrum at scales $10h^{-1} \geq D \geq 0.15h^{-1}$ Mpc with a precision of $\sim 15\%$. However at scales $\sim 3 - 150h^{-1}$ kpc the measured and CDM-like spectra are different. This result suggests a possible complex inflation with generation of excess power at small scales. Both confirmation of the CDM-like shape of the initial power spectrum or detection of its distortions at small scales are equally important for the widely discussed problems of physics of the early Universe, galaxy formation, and reheating of the Universe.

Key words: cosmology: large-scale structure of the Universe — quasars: absorption: general — surveys.

1 INTRODUCTION

One of the most perspective methods to study the processes responsible for the formation and evolution of the structure in the Universe is the analysis of properties of absorbers observed in spectra of the farthest quasars. The great potential of such investigations was discussed already by Oort (1981, 1984) just after Sargent et al. (1980) established the intergalactic nature of the Lyman- α forest. Indeed, the absorption lines trace the small scale distribution of hydrogen along the line of sight at redshifts $z \geq 2$ when matter is not yet strongly clustered and its observed characteristics can be

more easily interpreted. The available Keck and VLT high resolution observations of the Lyman- α forest provide a reasonable database and allow one to apply statistical methods for their analysis.

The composition and spatial distribution of the observed absorbers is complicated. Thus, at large redshifts the population of rich metal systems including Ly-damped and Ly-limit systems are rare and majority of observed absorbers is associated with isolated low mass HI clouds. At low redshifts a significant number of stronger Ly- α lines and metal systems is associated with galaxies (Bergeron et al. 1992; Lanzetta et al. 1995; Tytler 1995; Le Brune et al. 1996).

However as was recently shown by Penton, Stock and Shull (2000; 2002) and McLin et al. (2002), even at small redshifts some absorbers are associated with galaxy filaments while others are found within galaxy voids. These results suggest that the population of weaker absorbers dominating at higher redshifts can be associated with weaker structure elements formed by the non luminous baryonic and DM components. They also suggest that the Ly- α forest can be considered as a low mass component of the generic Large Scale Structure (LSS) which is seen in simulated and observed spatial matter distribution. This means that absorbers at high z trace the DM structure which is qualitatively similar to the rescaled one observed at small redshifts.

In this paper we investigate a sample of ~ 6000 absorbers observed in 19 high resolution spectra of QSOs and compare their properties with the improved model of absorbers proposed in Demiański & Doroshkevich (2003 a,b, hereafter Paper I & Paper II). We assume that absorbers are dominated by long-lived gravitationally bound and partially relaxed clouds composed of both DM and baryonic components. The fact that we can observe galaxies and quasars at $z \geq 3$ demonstrates the existence of strong density perturbations already then. Here we show that at these redshifts there are also strong negative density perturbations of a galactic scale which can be identified with rapidly expanded underdense regions. Such regions are naturally associated with the colder absorbers.

Our model explains the self similar character of evolution of the observed Doppler parameter, HI column density and absorber separation. Such evolution implies that the mean values of these characteristics slowly vary with redshift while their probability distribution functions (PDFs) remain unchanged. This model links the observed and other physical characteristics of absorbers – such as their DM column density, size, and fraction of matter associated with absorbers – and allows us also to identify several subpopulations of absorbers with different evolutionary histories.

We treat the evolution of structure as a random process of formation and merging of Zel'dovich pancakes, their transverse expansion and/or compression and successive transformation into filaments and high density clouds. Later on the hierarchical merging of pancakes, filaments and clouds forms rich galaxy walls observed at small redshifts. Impact of these factors is clearly seen in high resolution numerical simulations of evolution of the LSS (for review see, e.g. Frenk 2002).

Theoretical expectations of our model are based on the Zel'dovich approximate theory of gravitational instability (Zel'dovich 1970; Shandarin & Zel'dovich 1988). As is well known, it correctly describes only the linear and weakly nonlinear stages of the structure formation and cannot describe later stages of evolution of structure elements. In spite of this, the statistical approach proposed in (Demiański & Doroshkevich 1999, 2004a; hereafter DD99 & DD04) nicely describes the main properties of observed and simulated LSS (Demiański et al. 2000; Doroshkevich, Tucker, Allam & Way 2004) without any smoothing or filtering procedure.

Presently various observations are used to determine the power spectrum of the initial density perturbations. Its amplitude and its shape on scales $\geq 10h^{-1}$ Mpc are approximately established by investigations of the microwave relic radiation (Spergel et al. 2003, 2006) and the structure of the

Universe at $z \ll 1$ detected in large redshift surveys (Percival et al. 2001; Tegmark, Hamilton & Xu 2003; Verde et al. 2002, 2003) and weak lensing data (see, e.g., Hoekstra, Yee & Gladders 2002).

The shape of the initial power spectrum on scales $10h^{-1}$ Mpc – $1h^{-1}$ Mpc can be tested at high redshifts where it is not yet strongly distorted by nonlinear evolution (Croft et al. 1998, 2002; Nusser & Haehnelt 2000; Gnedin & Hamilton 2002; Viel et al. 2004 a,b; Kim et al. 2004; McDonald et al. 2004; Seljak et al. 2004; Zaroubi et al. 2005). The method used in these papers is surprisingly universal and is successfully applied to spectra observed with both high and moderate resolution. It utilizes the measured transmitted flux only and does not require preliminary determination of column density, Doppler parameters and even discrimination of hydrogen and metal line systems (McDonald et al. 2004, Seljak et al. 2004). In spite of this, it successfully restores the CDM-like power spectrum down to scales $\sim 1h^{-1}$ Mpc. Recent results on reconstruction of the initial power spectrum are summarized and discussed in many papers (see, e.g., Tegmark and Zaldarriaga 2003; Wang et al. 2003; Zaldarriaga, Scoccimorro & Hui 2003; Peiris et al. 2003; Spergel et al. 2003,2006; Tegmark et al. 2004; McDonald et al. 2004, Seljak et al. 2004).

A straightforward method of reconstruction of the initial power spectrum from the observed characteristics of absorbers was proposed and tested in Paper II. This method can be used to recover the initial power spectrum down to unprecedentedly small scale. In contrast with previous investigations (Croft et al. 1998, 2002; Nusser & Haehnelt 2000; Viel et al. 2004b; McDonald et al. 2004) we analyze the separation between adjacent absorbers and their column density rather than the flux or smoothed density field. This means that our results are not restricted by the standard factors such as the Nyquist limit, the impact of nonlinear processes, the unknown matter distribution between absorbers or their peculiar velocities. This approach successfully complements investigations of the power spectrum mentioned above.

Here we improve the analysis discussed in Paper II by using a richer observed sample and a more refined model of absorbers. We use two independent methods of determination of the initial power spectrum. The first one is based on measurements of the separation between adjacent absorbers, while the second one, proposed in Paper II, uses measurements of the column density of absorbers. Both approaches allow one to determine the spectrum down to the scale of $\sim 5 - 10h^{-1}$ kpc. At scales $(0.15 - 10)h^{-1}$ Mpc our results coincide with those expected for the CDM-like power spectrum and Gaussian perturbations with the precision of $\sim 15\%$. However, we have found some evidence that at scales $\leq 0.15h^{-1}$ Mpc the initial power spectrum differs from the CDM-like one suggesting a complex inflation with generation of excess power at small scales. Such excess power accelerates the process of galaxy formation at high redshifts and can shift the epoch of reheating of the Universe to higher redshifts.

At present we have only limited information about the properties of the background gas and the UV radiation (Haardt & Madau 1996; Scott et al. 2000, 2002; Schaye et al. 2000; McDonald & Miralda-Escude 2001; McDonald et al. 2000, 2001; Theuns et al. 2002 a, b; Levshakov et al. 2003; Boksenberg, Sargent & Rauch 2003; Demiański &

Doroshkevich 2004b) and therefor some numerical factors in our model remain undetermined. This means that our approach should be tested on representative numerical simulations that more accurately follow the process of formation and disruption of pancakes and filaments and provide a unified picture of the process of absorbers formation and evolution (see, e.g., Weinberg et al. 1998; Zhang et al. 1998; Davé et al. 1999; Theuns et al. 1999, 2000). But so far such simulations are performed mainly in small boxes what restricts their representativity, introduces artificial cutoffs in the power spectrum and complicates the quantitative description of structure evolution (see more detailed discussion in Gnedin & Hamilton 2002; Tegmark & Zaldarriaga 2002; Zaldarriaga Scoccimoro & Hui 2002; Seljak, McDonald & Makarov 2003; Manning 2003; Paper II). As was shown by Meiksin, Bryan & Machacek (2001), the available simulations reproduce quite well the characteristics of the flux but cannot restore other observed characteristics of the forest. This means that first of all numerical simulations should be improved (see more detailed discussion in Paper II).

Comparison of results obtained in Paper I and Paper II and in this paper demonstrates that the quality and representativity of the sample of observed absorbers are very important for the reconstruction of processes of absorbers formation and evolution. Thus, richer sample of the observed absorbers makes it possible to select and investigate several representative subsamples of absorbers with different evolutionary histories. None the less, our analysis indicates a possible deficit of weaker absorbers and pairs of close absorbers what in turn could be related to insufficient sensitivity of the process of absorbers' identification. Thus, the number and parameters of absorbers identified for the same quasar depend upon the used identification procedure. Further progress can be achieved first of all with richer samples covering the range of redshifts at least up to $z \sim 5$ what would allow one to perform a complex investigation of the early period of structure evolution.

This paper is organized as follows. In Sec. 2 the observational databases used in our analysis are presented and statistical characteristics of the observed parameters of absorbers are obtained. The theoretical models of the structure evolution are discussed in Sec. 3. The results of statistical analysis of the model dependent parameters and the derived initial power spectrum are given in Sec. 4. Discussion and conclusions can be found in Sec. 5.

2 OBSERVED CHARACTERISTICS OF ABSORBERS

2.1 Properties of the homogeneously distributed matter

In this paper we consider the spatially flat Λ CDM model of the Universe with the Hubble parameter and mean density given by:

$$H^2(z) = H_0^2 \Omega_m (1+z)^3 [1 + \Omega_\Lambda / \Omega_m (1+z)^{-3}],$$

$$\langle n_b(z) \rangle = 2.4 \cdot 10^{-7} (1+z)^3 (\Omega_b h^2 / 0.02) \text{cm}^{-3}, \quad (1)$$

$$\langle \rho_m(z) \rangle = \frac{3H_0^2}{8\pi G} \Omega_m (1+z)^3, \quad H_0 = 100h \text{ km/s/Mpc}.$$

Here $\Omega_m = 0.3$ & $\Omega_\Lambda = 0.7$ are the dimensionless matter density and the cosmological constant (dark energy), Ω_b is the dimensionless mean density of baryons, and $h = 0.7$ is the dimensionless Hubble constant.

Properties of the compressed gas can be suitably related to the parameters of homogeneously distributed gas, which were discussed in many papers (see, e.g., Ikeuchi & Ostriker 1986; Haardt & Madau 1996; Hui & Gnedin 1997; Scott et al. 2000; McDonald et al. 2001; Theuns et al. 2002a, b; Demiański & Doroshkevich 2004b). In this paper we consider evolution of absorbers at observed redshifts $z \leq 4$ when weak variations of the gas entropy are determined by the interaction of the gas with the UV background. Thus, the expected intensity of the UV background radiation, can be fitted as follows:

$$J(z, \nu) = J_{21}(z) \left(\frac{\nu_H}{\nu} \right)^{\alpha_\gamma} \cdot 10^{-21} \frac{\text{erg}}{\text{s cm}^2 \text{ sr Hz}}, \quad (2)$$

where $\nu_H = 3.3 \cdot 10^{15}$ Hz, $\alpha_\gamma \approx 1.5$ and the dimensionless factor $J_{21}(z)$ describes redshift variations of the intensity. The mean temperature, $\langle T_{bg} \rangle$, of homogeneous gas can be taken as

$$\langle T_{bg} \rangle \approx 3.5 z_4^{6/7} \Theta_{bg}^{4/7} \cdot 10^4 K,$$

$$\langle b_{bg} \rangle = \sqrt{\frac{2k_B \langle T_{bg} \rangle}{m_H}} \approx 24 z_4^{3/7} \Theta_{bg}^{2/7} \text{ km/s}, \quad (3)$$

$$\Theta_{bg} = \frac{\Omega_b h^2}{0.02} \frac{3.5}{2 + \alpha_\gamma} \left(\frac{0.15}{\Omega_m h^2} \right)^{3/4}, \quad z_4 = \frac{1+z}{4},$$

where k_B & m_H are the Boltzmann constant and the mass of the hydrogen atom and α_γ is the power index of spectrum of the ionizing background in (2). Analyzing the observed characteristics of absorbers McDonald et al. (2001) estimate the background temperature as $T_{bg} \approx (2 \pm 0.2) \cdot 10^4 K$ at $z \sim 2$, what is close to (3).

At this period the gas entropy can be characterized by the function

$$\langle F_{bg} \rangle = \frac{\langle T_{bg} \rangle}{\langle n_b \rangle^{2/3}} = 60 z_4^{-8/7} \Theta_{bg}^{4/7} \left(\frac{0.02}{\Omega_b h^2} \right)^{2/3} \text{ keV} \cdot \text{cm}^2. \quad (4)$$

As was shown in Demiański & Doroshkevich (2004b), the function $F_{bg} \propto (n_b / \langle n_b \rangle)^{0.1}$ only weakly depends upon variations of the expansion rate. This means that the background temperature and Doppler parameter vary as

$$T_{bg} \propto (n_b / \langle n_b \rangle)^{2/3}, \quad b_{bg} \propto (n_b / \langle n_b \rangle)^{1/3}, \quad (5)$$

and the mildly nonlinear compression or expansion of matter occurs almost adiabatically. Thus, within compressed or slowly expanded regions with $n_b \geq \langle n_b \rangle$ we can expect that $T_{bg} \geq \langle T_{bg} \rangle$ while in rapidly expanded regions with $n_b \ll \langle n_b \rangle$ we can expect that $T_{bg} \ll \langle T_{bg} \rangle$.

Under the assumption of ionization equilibrium of the gas,

$$\frac{\langle n_H \rangle}{\langle n_b \rangle} = \frac{\alpha_r \langle n_b \rangle}{\Gamma_\gamma}, \quad \alpha_r \approx 4.4 \cdot 10^{-13} \left(\frac{10^4 K}{T} \right)^{3/4} \frac{\text{cm}^3}{\text{s}}, \quad (6)$$

where $\alpha_r(T)$ is the recombination coefficient (Black, 1981) and Γ_γ characterizes the rate of ionization by the UV background, the fraction of neutral hydrogen is

$$x_{bg} = \langle n_H \rangle / \langle n_b \rangle = x_0 (1+z)^{33/14}, \quad (7)$$

Table 1. QSO spectra used in our analysis

	z_{em}	z_{min}	z_{max}	No of HI lines
1055 + 461 ¹	4.16	2.8	4.16	998
0000 – 260 ²	4.11	3.4	4.1	431
0055 – 259 ³	3.66	3.0	3.6	534
1422 + 23 ¹	3.6	2.7	3.6	811
0014 + 813 ⁴	3.41	2.7	3.2	262
0956 + 122 ⁴	3.30	2.6	3.1	256
0302 – 003 ^{4,3}	3.29	2.6	3.1	356
0636 + 680 ¹	3.17	2.5	3.0	531
0636 + 680 ⁴	3.17	2.4	3.1	313
1759 + 754 ⁵	3.05	2.4	3.0	307
1946 + 766 ⁶	3.02	2.4	3.0	461
1107 + 485 ¹	3.0	2.1	3.0	609
1347 – 246 ³	2.63	2.1	2.6	361
1122 – 441 ³	2.42	1.9	2.4	353
2217 – 282 ³	2.41	1.9	2.3	262
1626 – 643 ¹	2.32	1.5	2.3	281
2233 – 606 ⁷	2.24	1.5	2.2	293
1101 – 264 ³	2.15	1.6	2.1	277
0515 – 441 ³	1.72	1.5	1.7	76

1. Rough & Sargent, unpublished 2. Lu et al. (1996), 3. Kim et al. 2002 4. Hu et al., (1995), 5. Djorgovski et al. (2001) 6. Kirkman & Tytler (1997), 7. Cristiani & D’Odorico (2000),

$$x_0 \approx \frac{1.2 \cdot 10^{-7} \Omega_b h^2}{\Gamma_{12}(z)} \Theta_{bg}^{-3/7}, \quad \Gamma_\gamma(z) = 10^{-12} \Gamma_{12}(z) s^{-1},$$

$$\Gamma_{12}(z) = 12.6 J_{21}(z) (3 + \alpha_\gamma)^{-1}.$$

The redshift variations of the rate of ionization, $\Gamma_{12}(z)$, produced by the UV radiation of quasars were discussed by Haardt & Madau (1996) and later on tested and corrected by Demiański & Doroshkevich (2004b) with large observed sample of QSOs. For $\alpha_\gamma \approx 1.5$ the expected ionization rate of hydrogen is fitted by the expression:

$$\Gamma_{12} \approx 7 \exp[-(z - 2.35)^2/2]. \quad (8)$$

Variations of the power index α_γ with time and space generate random variations of Γ_{12} . With these parameters of background we have for the Gunn–Peterson optical depth

$$\tau_{GP}(z) \approx \frac{0.34}{\Gamma_{12} \Theta_{bg}^{3/7}} \left(\frac{1+z}{4}\right)^{27/7} \left(\frac{\Omega_b h^2}{0.02}\right)^2 \sqrt{\frac{0.15}{\Omega_m h^2}}, \quad (9)$$

$$\tau_{GP}(2) \approx 0.015, \quad \tau_{GP}(5) \approx 8.2.$$

However these estimates of Γ_{12} should be corrected for absorption and reemission of radiation within high density clouds (Haardt & Madau 1996). This effect decreases the ionization rate of both hydrogen and helium and enhances a possible spatial variations of intensity of the UV background. According to the observational estimates of Scott et al. (2002) $\Gamma_{12} \sim 1-4$ at $z \approx 2$ (see also Levshakov et al. 2003; Boksenberg, Sargent & Rauch 2003). On the other hand, Eq. (8) takes into account only the contribution of QSOs and, so, it underestimates the ionization rate at both $z \leq 2$ and $z \geq 3$ where contribution of other probable sources of radiation becomes important.

2.2 The database.

The present analysis is based on 19 high resolution spectra listed in Table 1. These spectra contain 7 770 absorbers. For further discussion we selected the sample of 7 430 absorbers with $11.9 \leq \lg N_{HI} \leq 15$ and 7 411 distances between neighboring absorbers. This sample will be used for discussion of the correlation function of initial velocity field. For detailed investigation we selected a more homogeneous sample of 6 270 absorbers and 6 251 separations with $b \geq 5 \text{ km/s}$ and we restricted errors of measurement by the conditions $\Delta \lg N_{HI} \leq 0.2$ and $\Delta b \leq 0.3b$. The chosen low limit of b is close to the spectral resolution in this sample. To test the sample dependence of the correlation function of initial velocity field we use for comparison the sample of 14 QSOs with 4 036 absorbers investigated in Paper I and Paper II.

However, a list of absorbers depends also upon the method of line identification and, for example, for QSO 0636+680 two spectra listed in Table 1 include different number of absorbers. This example shows that the methods of line identification should be unified and improved. None the less, dispersions of absorbers characteristics discussed below are defined mainly by their broad distribution functions and by the completeness of the samples. Because of this, in this paper we discuss the scatter of only the more interesting quantitative characteristics of absorbers.

As is seen from Fig. 1, the redshift distribution of absorbers is non homogeneous and the majority of absorbers are concentrated at $2 \leq z \leq 3.5$. This means that some of the discussed here characteristics of absorbers are derived mainly from this range of redshifts. Absorbers at $z \geq 3.5$ were identified mainly in spectra of QSOs 0000-260 and 1055+461. In this range and at $z \leq 2$ the statistics of lines is not sufficient.

2.3 Observed characteristics of absorbers

For the sample of 6 270 absorbers the redshift variations of the three mean observed characteristics of absorbers, namely, the Doppler parameter, $\langle b \rangle$, the column density of neutral hydrogen, $\langle \lg N_{HI}^* \rangle = \langle \lg(N_{HI}/z_4^2) \rangle$, and the mean separation of absorbers, $\langle d_{sep}^* \rangle = \langle d_{sep} z_4^2 \rangle$, $z_4 = (1+z)/4$ are plotted in Fig. 1 for $1.6 \leq z \leq 4$. These variations are well fitted by

$$\langle \lg N_{HI}^* \rangle = \langle \lg(N_{HI}/z_4^2) \rangle = 13.3 \pm 0.08,$$

$$\langle b \rangle = (26 \pm 2.1) \text{ km/s}, \quad z_4 = (1+z)/4, \quad (10)$$

$$\langle d_v^* \rangle = \langle 2b/H(z) z_4^{3/2} \rangle = (0.12 \pm 0.01) h^{-1} \text{ Mpc},$$

$$\langle d_{sep}^* \rangle = \langle d_{sep} z_4^2 \rangle = (1.3 \pm 0.15) h^{-1} \text{ Mpc},$$

respectively. For the sample of 7 411 separations we get

$$\langle d_{sep}^* \rangle = (1 \pm 0.1) h^{-1} \text{ Mpc}.$$

Detailed discussion of the observed characteristics of absorbers can be found, for example, in Kim, Cristiani & D’Odorico (2002), Kim et al. (2002, 2004).

The observed probability distribution functions, PDFs, for the Doppler parameter, $P(b)$, the hydrogen column density, $P(N_{HI}/z_4^2)$, and the absorbers separation, $P(d_{sep} z_4^2)$, are plotted in Fig. 2. Such choice of variables allows us to suppress the redshift evolution of the mean characteristics

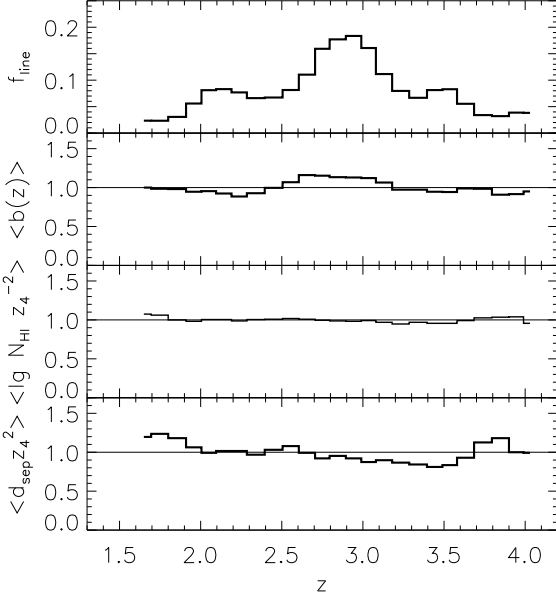


Figure 1. Redshift variations of fraction of measured absorbers, $f_{line} = \Delta N_{abs}(z)/N_{abs}$, (top panel), mean Doppler parameter, $\langle b(z) \rangle$ and HI column density, $\langle \lg(N_{HI} z_4^{-2}) \rangle$ (two middle panels), and the mean absorber separation, $\langle d_{sep} z_4^2 \rangle$ (bottom panel). All functions are normalized over the mean values given by (10).

of absorbers. PDFs for so corrected parameters only weakly vary with redshift and, as was discussed in Paper I, for the main fraction of absorbers, these variations do not exceed 10 – 15%. These PDFs are well fitted by exponential functions

$$P_{fit}(x_{HI}) \approx 0.4 \exp(-0.8x_{HI}) + 2.9 \exp(-5x_{HI}),$$

$$P_{fit}(x_b) \approx \begin{cases} 0.15 \exp(2.8x_b), & b \leq b_{rap}, \\ 0.9 \exp(-2.3x_b), & b \geq b_{rap}, \end{cases} \quad (11)$$

$$P_{fit}(x_s) \approx 3.5 \exp(-1.8x_s) \text{erf}^4(\sqrt{1.8x_s})/\sqrt{x_s},$$

$$x_b = \frac{b}{\langle b \rangle}, \quad x_{HI} = \frac{N_{HI}/z_4^2}{\langle N_{HI}/z_4^2 \rangle}, \quad x_s = \frac{d_{sep} z_4^2}{\langle d_{sep} z_4^2 \rangle} = \frac{d_{sep}^*}{\langle d_{sep}^* \rangle},$$

where again $z_4 = (1+z)/4$ and $b_{rap} \approx 23.5 \text{ km/s} \sim \langle b_{bg} \rangle$ (3) discriminates between absorbers situated in the increasing and decreasing parts of the PDF $P(x_b)$ in Fig. 2. The similarity of b_{rap} and $\langle b_{bg} \rangle$ is an independent confirmation of estimates (3). For the scatter of measured PDF, $P(x_s)$, around the fit (11) we have

$$P_{fit}(x_s)/P(x_s) \approx 1.04 \pm 0.15, \quad x_s \leq 2. \quad (12)$$

Any model of the forest has problems explaining the complex shape of the observed PDF $P(x_b)$ and the existence of absorbers with $b \leq b_{bg}$. These absorbers are sometimes related to the unidentified metal lines what is perhaps possible for colder absorbers. However, large fraction of such absorbers ($\sim 40\%$) indicates that majority of them must be related to usual hydrogen clouds formed within regions with lower background temperature. Our analysis shows that statistical characteristics of these absorbers are consistent with expected ones for absorbers formed due to adiabatic compression in rapidly expanded regions (see Secs. 3.5 & 4.5). Examples of such absorbers were also found in simulations (see, e.g., Bi & Davidsen 1997; Zhang et al. 1998; Davé et

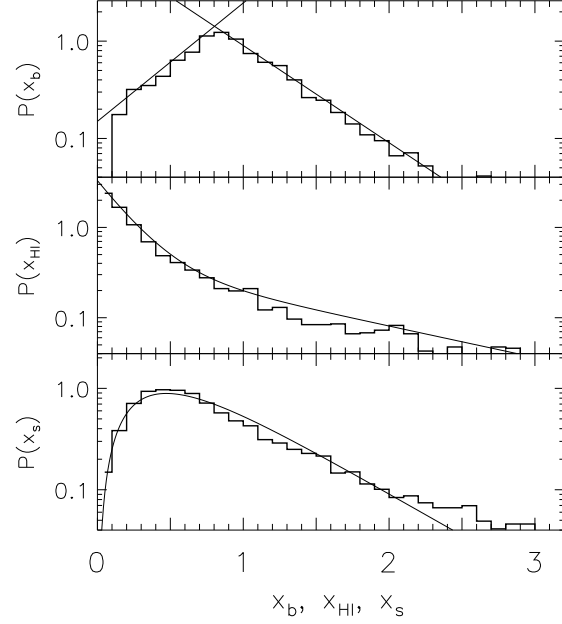


Figure 2. Observed PDFs for the Doppler parameter, $P(x_b)$, the hydrogen column density, $P(x_{HI})$, and absorbers separations, $P(x_s)$, are plotted together with fits (11) (solid lines).

al. 1999). This subpopulation can also contain some number of "artificial" caustics (McGill 1990).

The mean size of rapidly expanded regions, $\langle D_{rap} \rangle$, can be measured as a distance along the line of sight between two absorbers with $b \geq b_{rap}$ closest to a colder absorber. It increases with time as

$$\langle D_{rap} z_4^2 \rangle \approx 1.6 \pm 0.2 h^{-1} \text{ Mpc}, \quad (13)$$

and the typical mass associated with these regions is

$$M_{rap} \sim \frac{\pi}{6} \langle \rho(z) \delta_m D_{rap}^3 \rangle \sim 10^{13} z_4^{-3} \langle \delta_m \rangle M_{\odot} \left(\frac{\Omega_m 0.7}{0.3 h} \right), \quad (14)$$

where $\delta_m = \rho_m / \langle \rho_m \rangle \leq 1$. At $z_4 \sim 1$ the mass M_{rap} is in the range of galactic masses and it rapidly increases with time. This result is consistent with the expected symmetry of positive and negative initial density perturbations what leads to formation of both galaxies and rapidly expanded regions.

Even these results allow one to obtain some inferences on the evolution of the forest:

(i) Regular redshift variations of the mean observed characteristics of absorbers (10) and weak redshift dependence of PDFs (11) indicate the self similar character of absorber's evolution over the whole range of redshifts under consideration. So, we can conclude, that at these redshifts the evolution is dominated by a balanced action of the same physical factors.

(ii) The complex form of the PDF $P(b)$ confirms that absorbers have been formed within both rapidly and moderately expanded regions. Analysis of these subpopulations of absorbers allows one to estimate some parameters of such regions. We will discuss this problem in Secs. 3.5 & 4.5.

(iii) The very wide range of measured Doppler parameters, $0.2 \leq b/b_{bg} \leq 5$, indicates a wide variety of initial perturbations. Such a wide range of Doppler parameters is not reproduced in simulations (Meiksin et al. 2001).

(iv) The decline of the measured $\langle N_{HI} \rangle \propto (1+z)^2$ could be related to the retained expansion of majority of observed absorbers in the transverse directions.

(v) The growth of the mean observed separation between absorbers, $\langle d_{sep} \rangle \propto (1+z)^{-2}$ indicates the progressive decline of the number density of observed absorbers that can be related to the decrease of their hydrogen column density under the observational limit $N_{HI} \approx 10^{12} \text{ cm}^{-2}$.

(vi) Comparison of measured $\langle d_v(z) \rangle$ and $(1+z)^{-1} \langle d_{sep}(z) \rangle$ (10) indicates that at $z \geq 4$ the expected overlapping of absorbers becomes essential and, perhaps, absence of observed absorbers in spectra of the farthest QSO (Fan et al. 2002, 2003, 2004) can be partly related to this effect.

3 MODEL OF ABSORBERS FORMATION AND EVOLUTION

3.1 Physical model of absorbers

Many models were proposed during the last twenty years to explain regular redshift variations of the mean observed characteristics of absorbers (10) and weak redshift dependence of PDFs (11) (see references in Rauch (1998), and in Paper I and Paper II). The simplest one connects the absorber characteristics with a suitable set of early formed equilibrium clouds. This model naturally explains the weak redshift dependence of the mean Doppler parameter, $\langle b \rangle$, and the observed PDFs (11). It explains also the regular redshift variations of the mean absorber separation (10). Indeed, the mean proper free path between absorbers is

$$(1+z)^{-1} \langle d_{sep}(z) \rangle \propto (1+z)^{-3} \propto \langle n_{abs}(z) S_{abs}(z) \rangle^{-1}, \quad (15)$$

where n_{abs} & S_{abs} are the number density and the surface area of such clouds orthogonal to the line of sight. In this case we have from (15)

$$n_{abs}(z) \propto (1+z)^3, \quad S_{abs}(z) \propto const(z).$$

However, it is well known that the existence of such low density equilibrium clouds cannot be reasonably explained. Moreover, with this model the observed evolution of the mean column density of neutral hydrogen, $\langle N_{HI} \rangle \propto (1+z)^2$, must be related to the monotonic evolution of the UV background, $\langle \Gamma_{12} \rangle \propto (1+z)^{-2}$, what disagrees with the available estimates of Γ_{12} .

Numerous simulations indicate that the majority of the LSS elements can be related to the extended anisotropic moderate density clouds with a complex internal structure and low density envelope. Such long lived clouds are relaxed along the shorter axis and are expanded/compressed along transverse directions. The formation of DM pancakes as an inevitable first step of evolution of small perturbations was firmly established both by theoretical considerations (Zel'dovich 1970; Shandarin & Zel'dovich 1989) and numerical simulations (Shandarin et al. 1995). The anisotropic galaxy walls such as the Great Wall are observed in the SDSS and 2dF galaxy surveys and represent examples of the Zel'dovich pancakes. This suggests that absorbers can also be linked with the Zel'dovich pancakes and the reasonable model of the forest evolution can be constructed on the basis of the Zel'dovich theory.

However, in some papers devoted to the hydrodynamical simulations of the forest evolution absorbers are often identified with unrelaxed moderate density clouds and their Doppler parameter b is related to the gradient of velocity of infalling matter rather than to thermal velocities. Of course, observed samples include some fraction of such objects mainly among weaker absorbers. However, properties of richer absorbers with metal systems are found to be in a good agreement with a model assuming local hydrostatic equilibrium (see, e.g. Carswell, Schaye & Kim 2002; Telfer et al. 2002; Simcoe, Sargent, Rauch 2002, 2004; Boksenberg, Sargent, Rauch 2003; Manning 2002, 2003 a,b; Bergeron & Herbert-Fort 2005). This means that, possibly, the fraction of simulated extended unrelaxed clouds is artificially enhanced by technical limitations (see, e.g., discussion in Meiksin, Bryan & Machacek 2001; Manning 2003 and Paper II). It is important that these simulations cannot yet reproduce well enough the characteristics of observed absorbers discussed in previous Section.

This discussion shows that an adequate physical model of the complex evolution of the forest has not been proposed yet. Indeed, the relaxation of DM pancakes leads to complex internal structure of pancakes, the adiabatic compression and/or expansion of absorbers in transverse directions is changing their overdensity and temperature, the radiative cooling and bulk heating leads to the drift of the gas entropy and overdensity but leaves unchanged the depth of the potential well formed by DM distribution. Merging of pancakes increases more strongly the depth of the potential well and the gas entropy but the overdensity of the gaseous component increases only moderately. The temperature and overdensity of the trapped gas are rearranged in accordance with the condition of hydrodynamic equilibrium across the pancake continuously. These processes imply the existence of a complicated time-dependent internal structure of absorbers.

In this paper we discuss the model of absorbers evolution based on the Zel'dovich theory. This analytical model links the self similar evolution of dominated DM component with observed characteristics of absorbers. Here we assume that:

(i) The DM distribution forms a set of sheet-like clouds (Zel'dovich pancakes), their basic parameters are approximately described by the Zel'dovich theory of gravitational instability applied to the CDM or WDM initial power spectrum (DD99; DD04). The majority of DM pancakes are partly relaxed, long-lived, and their properties vary due to the successive accretion of matter, merging and expansion and/or compression in the transverse directions.

(ii) Gas is trapped in the gravitational potential wells formed by the DM distribution. For majority of absorbers, the observed Doppler parameter, b , traces the gas temperature and the depth of the DM potential wells. We consider the possible macroscopic motions within pancakes as subsonic and assume that they cannot essentially distort the measured Doppler parameter.

(iii) The gas is ionized by the UV background and for the majority of absorbers ionization equilibrium is assumed.

(iv) For a given temperature, the gas density within the potential wells is determined by the gas entropy created during the previous evolution. The gas entropy is changing,

mainly, due to relaxation of the compressed matter, shock heating in the course of merging of pancakes, bulk heating by the UV background and local sources and due to radiative cooling. These processes slowly change the entropy and density of the trapped gas. Random variations of the intensity and spectrum of the UV background enhance random scatter of the observed properties of absorbers.

In this model we expect that the mean surface density of both DM and baryonic components of pancakes weakly varies with time and the mean density of matter compressed within absorbers decreases as $\langle \rho_{abs} \rangle \propto (1+z)^v$, $v \sim 1.5 - 1$ for colder and hotter absorbers, respectively. We cannot discriminate between evolution of the absorbers number density, n_{abs} , and their surface area, S_{abs} . However, numerical simulations demonstrate that the general tendency of evolution is a sequential growth of masses and sizes of pancakes accompanied by a drift of weaker ones under the observational limit and decrease of the comoving number density of observed absorbers. Thus, as is seen from (15), if the surface area of absorbers increases $\langle S_{abs} \rangle \propto (1+z)^{-\kappa}$ then the number density of observed absorbers decreases as $\langle n_{abs} \rangle \propto (1+z)^{3+\kappa}$. We show that the observed evolution of mean hydrogen column density and mean absorber separations (10 & 11) coincides with theoretical expectations for Gaussian initial perturbations.

The wide range of the observed Doppler parameters, $5-10 \text{ km/s} \leq b \leq 100 \text{ km/s}$, demonstrates a complex composition of the forest. In this paper we roughly identify three subpopulations of absorbers, namely, hot absorbers formed in the course of merging and shock compression, warm absorbers formed due to adiabatic and weak shock compression in moderately expanded regions, and an unexpectedly rich subpopulation of colder absorbers. We link the measured Doppler parameter with the depth of 1D potential well formed by the compressed DM component and we neglect the contribution of macroscopic velocities what restricts the achieved precision of our approach. Non the less this model reproduces quite well the self similar evolution of absorbers and allows one to reconstruct the initial correlation function of velocities and the initial power spectrum down to very small scales.

3.2 The initial power spectrum and correlation functions of the initial velocity field

In this Section we summarize the main results obtained in DD99 and DD04 concerning the evolution of DM pancakes and in Sec. 3.9 we show how to improve the estimates of the correlation function of the initial velocity field, and the shape of initial power spectrum discussed in Paper II.

As a reference power spectrum of initial perturbations we take the standard CDM-like spectrum with the Harrison – Zel’dovich asymptotic,

$$P(k) = \frac{A^2 k}{k_0^4} T^2(\eta) D_W(\eta), \quad \eta = \frac{k}{k_0}, \quad k_0 = \frac{\Omega_m h^2}{\text{Mpc}}, \quad (16)$$

where A is the dimensionless amplitude of perturbations, k is the comoving wave number. The transfer function, $T(\eta)$, and the damping factor, $D_W(\eta)$, describing the free streaming of DM particles were given in Bardeen et al. (1986). For

WDM particles the dimensionless damping scale, R_f , and the damping factor, D_W , are

$$R_f = \frac{1}{5} \left(\frac{\Omega_m h^2 \text{keV}}{M_{DM}} \right)^{4/3}, \quad D_W = \exp[-\eta R_f - (\eta R_f)^2],$$

where M_{DM} is the mass of WDM particles in keV (Bardeen et al. 1986). This relation illustrates the clear dependence of characteristics of small scale perturbations on the mass of DM particles.

For the spectrum (16) the coherent lengths of velocity and density fields, l_v & l_ρ , are expressed through the spectral moments, m_{-2} & m_0 , (DD99) as follows:

$$l_v = \frac{1}{k_0 \sqrt{m_{-2}}} = \frac{6.6}{\Omega_m h^2} \text{Mpc} \approx 31.4 h^{-1} \frac{0.21}{\Omega_m h} \text{Mpc}, \quad (17)$$

$$m_{-2} = \int_0^\infty d\eta \eta T^2(\eta) D_W(\eta) \approx 0.023, \quad l_\rho = q_0 l_v,$$

$$m_0 = \int_0^\infty d\eta \eta^3 T^2(\eta) D_W(\eta), \quad q_0 = 5 \frac{m_{-2}^2}{m_0}.$$

The moment m_0 depends upon the mass of dominant component of DM particles and as is shown in Sec. 4.2, $q_0 \leq 10^{-3}$, $m_0 \geq 2.4$, $M_{DM} \geq 1 \text{ MeV}$.

As was demonstrated in DD99 and DD04, the basic statistical characteristics of structure are expressed through the normalized longitudinal correlation function of the initial velocity field, $\mathbf{v}(\tilde{\mathbf{q}})$,

$$\xi_v(l_v q) = 3 \frac{\langle (\mathbf{q} \cdot \mathbf{v}(\tilde{\mathbf{q}}_1)) (\mathbf{q} \cdot \mathbf{v}(\tilde{\mathbf{q}}_2)) \rangle}{\sigma_v^2 q^2}, \quad \mathbf{q} = \frac{\tilde{\mathbf{q}}_1 - \tilde{\mathbf{q}}_2}{l_v}. \quad (18)$$

Here $\tilde{\mathbf{q}}_1$ & $\tilde{\mathbf{q}}_2$ are the unperturbed coordinates of two particles at $z = 0$, $q = |\mathbf{q}|$, and σ_v^2 is the velocity variance. This function is expressed through the power spectrum:

$$\xi_v(l_v q) = \frac{3}{m_{-2}} \int_0^\infty d\eta \eta^2 \cos x \int_\eta^\infty \frac{dy}{y^2} T^2(y) D_W(y), \quad (19)$$

$$\eta T^2(\eta) D_W(\eta) = \frac{\sqrt{m_{-2}}}{3} \int_0^\infty (2 \cos x + x \sin x) \xi_v(l_v q) dq,$$

$$x = kl_v q, \quad \eta = k/k_0, \quad \xi_v(0) = 1, \quad \int_0^\infty dq \xi(l_v q) = 0.$$

Similar relations can be also written for any initial power spectrum $P(k)$.

For the CDM – like spectrum (16) with $q_0 < 10^{-3}$ and for the most interesting range $0.5 \geq q$ the velocity correlation function can be fitted as follows:

$$\xi_v(q) = \xi_{CDM} \approx 1 - \frac{1.5q^2}{\sqrt{2.25q^4 + q^2 + p_0^{1.4} q^{0.6} + q_0^2}}, \quad (20)$$

where $p_0 \approx 1.1 \cdot 10^{-2}$ and q_0 was introduced in (17). Further on, we will use this function as the reference one and will compare it with observational estimates of $\xi_v(q)$.

As was shown in DD99 and DD04, the main DM characteristics depend upon the self similar variable

$$\zeta(q, z) = \frac{q^2}{4\tau^2(z)[1 - \xi_v(q)]}, \quad (21)$$

where the ‘time’ $\tau(z)$ describes the growth of perturbations due to the gravitational instability. For the Λ CDM cosmo-

logical model (1), and for $z \geq 2$ we have

$$\tau(z) \approx \tau_0 \left(\frac{1 + 1.2\Omega_m}{2.2\Omega_m} \right)^{1/3} \frac{1}{1+z} \approx \frac{1.27\tau_0}{1+z}, \quad (22)$$

and τ_0 characterizes the amplitude of initial perturbations. It is proportional to σ_8 , the variance of the mass within a randomly placed sphere of radius $8h^{-1}\text{Mpc}$. Latest estimates (Spergel et al. 2003, 2006; Viel et al. 2004b) for the model (1) are

$$\sigma_8 \approx 0.9 \pm 0.1, \quad \tau_0 = 0.21\sigma_8 \approx (0.19 \pm 0.02) \frac{\sigma_8}{0.9}. \quad (23)$$

3.3 Expected characteristics of DM absorbers

In this section we introduce (without proofs) the basic characteristics of DM pancakes as a basis for further analysis. For more details see DD99 and DD04.

3.3.1 DM column density of absorbers

The fundamental characteristic of DM pancakes is the dimensional, μ , or the dimensionless, q , Lagrangian thickness (the dimensionless DM column density) :

$$\mu \approx \frac{\langle \rho_m(z) \rangle l_v q}{(1+z)} = \frac{3H_0^2}{8\pi G} l_v \Omega_m (1+z)^2 q, \quad (24)$$

where l_v is the coherent length of initial velocity field (17). The Lagrangian thickness of a pancake, $l_v q$, is defined as the unperturbed distance at redshift $z = 0$ between DM particles bounding the pancake (18).

As was found in DD99 and DD04 for Gaussian initial perturbations, the expected probability distribution function for the DM column density is

$$N_q(\zeta) \approx \frac{2}{\sqrt{\pi}} e^{-\zeta} \frac{\text{erf}(\sqrt{\zeta})}{\sqrt{\zeta}}, \quad W_q(< \zeta) = \text{erf}^2(\zeta), \quad (25)$$

$$\langle \zeta \rangle \approx \frac{1}{2} + \frac{1}{\pi} \approx 0.82, \quad \langle q \rangle \approx 6\tau^2 \langle \zeta \rangle \approx \frac{2 \pm 0.2}{z_4^2} 10^{-2} \left(\frac{\tau_0}{0.2} \right)^2,$$

where $z_4 = (1+z)/4$, $\zeta(q, z)$ was introduced in (21) and $W_q(< \zeta)$ is the cumulative probability function.

Strictly speaking, the relations (24) and (25) are valid for pancakes formed and observed at the same redshift $z_{obs} = z_f$ because after pancake formation the transverse expansion and compression changes its DM column density and other characteristics. However, owing to the symmetry of moderate distortions of general expansion in transverse directions, these processes do not change the statistical characteristics for majority of pancakes observed at redshift $z_{obs} \leq z_f$ (DD04). This means that statistically we can consider each pancake as created at the observed redshift. However, the symmetry is distorted for rapidly expanded regions observed as absorbers with $b \ll b_{bg}$ because the cross-section of strongly compressed absorbers is small and, therefore, they are rarely observed. More details are given in Secs. 3.5, 3.6 and in DD04.

3.3.2 Proper sizes of absorbers

The actual thickness of a DM pancake is estimated as

$$d_{abs} = \frac{\mu}{\rho_m} = \frac{l_v q}{(1+z)\delta_m}, \quad \delta_m = \rho_m / \langle \rho_m(z) \rangle. \quad (26)$$

Here δ_m is the mean overdensity of compressed matter above the background density.

For the transverse size of absorbers, the expected characteristics were estimated in DD04 as follows:

$$N_{tr}(\zeta_{tr}) \approx \frac{2}{\sqrt{\pi}} \exp(-\zeta_{tr}^2), \quad \zeta_{tr}^2 \approx \frac{q_{tr}}{6\tau^2(z)}, \quad (27)$$

$$\langle \zeta_{tr}^2 \rangle \approx 1/2, \quad \langle l_v q_{tr} \rangle \approx 3\tau^2(z) l_v \approx 0.45 z_4^{-2} h^{-1} \text{Mpc}.$$

Here again $z_4 = (1+z)/4$, z is the observed redshift and $l_v q_{tr}$ is the expected size of absorbers at $z = 0$.

3.3.3 Absorbers separation

An important characteristic of the distribution of absorbers is their separation determined as the distance along the line of sight between centers of neighboring absorbers observed with the separation Δz ,

$$d_{sep} = \frac{c\Delta z}{H(z)} = 5.5 \cdot 10^3 \frac{\Delta z}{(1+z)^{3/2}} \sqrt{\frac{0.3}{\Omega_m}} h^{-1} \text{Mpc}. \quad (28)$$

This separation is identical to the free path between absorbers and is quite similar to the popular descriptor

$$\frac{\Delta N_{abs}}{\Delta z} \propto \langle d_{sep}(z) \rangle^{-1}. \quad (29)$$

For Gaussian initial perturbations the PDF for the absorber separations in Lagrangian space, d_L , is

$$N_L(\zeta_L) \approx 4\pi^{-1/2} \exp(-\zeta_L) [(1+2\zeta_L) D_w(\sqrt{\zeta_L}) - \sqrt{\zeta_L}] \\ \approx 2.82 \exp(-\zeta_L) \text{erf}^4(\zeta_L) / \sqrt{\zeta_L}, \quad (30)$$

$$\zeta_L = \zeta(q_L, z), \quad q_L = d_L/l_v, \quad \langle \zeta_L \rangle \approx 1.5,$$

where $\zeta(q, z)$ was introduced by (21) and

$$D_w(x) = \int_0^x dy \exp(y^2 - x^2)$$

is the Dawson function.

Comparing the pancake surface density, $\mu(z)$, with the absorbers separation, d_{sep} , we can also estimate the fraction of matter accumulated by absorbers as

$$f_{abs} \simeq \frac{\mu(1+z)}{\langle \rho_m \rangle d_{sep}} = \frac{l_v q}{d_{sep}}, \quad \langle f_{abs} \rangle \approx \frac{\langle q \rangle}{\langle q_L \rangle} \approx 0.55. \quad (31)$$

However, this formal estimate is of limited significance because it does not consider the complex processes of absorbers evolution. More detailed 3D analysis (DD04) shows that at a later period of absorbers evolution we can expect

$$f_{abs} \simeq 0.38 - 0.44 \quad (32)$$

The observed characteristics of absorbers are measured in the redshift space where both the proper motions of absorbers and their peculiar velocities distort the PDF (30) and, in particular, lead to the merging and artificial blending of absorbers. These processes are driven by the spatial modulations of gravitational potential formed by the large scale perturbations and can be also described in the framework of Zel'dovich approximation (DD99). However, such description depends upon the size of absorbers (26) which variations with redshift cannot be described theoretically. So, characteristics of absorbers in both real and redshift spaces can be determined only approximately.

For the PDF of absorbers separation in the redshift space we get

$$N_{sep} \approx 2.4 \exp(-1.35x_{rd})[1 - 0.85 \exp(-1.35x_{rd})] \quad (33)$$

$$x_{rd} = \frac{\zeta(q_{rd}, z)}{\langle \zeta(q_{rd}, z) \rangle}, \quad \langle \zeta(q_{rd}, z) \rangle \approx 2.13, \quad q_{rd} = \frac{d_{sep}}{l_v},$$

$$\langle d_{sep} \rangle \approx 6l_v \tau^2 \langle \zeta(q_{rd}, z) \rangle \approx 1.3z_4^{-2} h^{-1} \text{Mpc} (\tau_0/0.2)^2,$$

where $z_4 = (1+z)/4$ and $\zeta(q, z)$ & d_{sep} are defined by (21) and (28). These expressions describe correctly properties of larger separations but become unreliable for smaller separations where the influence of the proper sizes of absorbers is more important. In the real space the expression (33) also approximates the PDF of distances between neighboring absorbers but the mean value $\langle \zeta_{real} \rangle \approx 1.64$ is smaller than that in the redshift space.

The same approach allows us to determine the expected characteristics of merged absorbers. Instead of (25), in redshift space, we get for such absorbers

$$N_{mrg}(x) \approx 1.3 \exp(-1.1x)[1 - 0.5 \exp(-2.2x)], \quad (34)$$

$$x = \zeta_{mrg} / \langle \zeta_{mrg} \rangle, \quad \zeta_{mrg} = \zeta(q_{mrg}, z), \quad \langle \zeta_{mrg} \rangle = 1.22,$$

where $\zeta(q, z)$ was introduced in (21) and q_{mrg} is the dimensionless DM column density of merged absorbers. This relation indicates that the population of poorer merged absorbers is suppressed and, in particular, the mean DM column density of merged absorbers is larger than that for all absorbers as given by (25).

The relations (25), (31), (33), (34) show that during the self similar period of structure evolution, when the relations (20) and (22) are valid, we can expect regular variations of the basic characteristics of absorbers such as their DM column density, q , separation, d_{sep} , and fraction of matter accumulated by absorbers, f_{abs} . These regular variations are distorted at small redshifts when the growth of perturbations is decelerated and at higher redshifts, when the blending of absorbers becomes more important.

3.4 Doppler parameters of absorbers

For relaxed and gravitationally confined absorbers their Doppler parameters are closely linked to the potential wells formed by the DM distribution. As is well known, for an equilibrium slab of DM the depth of its potential well is

$$\Delta\Phi \approx \frac{\pi G \mu^2}{\langle \rho(z) \rangle \delta_m} \Theta_\Phi = \frac{3}{8} v_0^2 \frac{q^2 (1+z)}{\delta_m} \Theta_\Phi, \quad (35)$$

$$v_0 = H_0 l_v \sqrt{\Omega_m} = 1720 \text{ km/s} \sqrt{\frac{0.15}{\Omega_m h^2}}.$$

where the random factor Θ_Φ characterizes the inhomogeneity of DM distribution across the slab and the evaporation of matter in the course of its relaxation.

Analysis of numerical simulations (Demiański et al. 2000) indicates that the relaxed distribution of DM component can be approximately described by the polytropic equation of state with the power index $\gamma_m \approx 1.5 - 2$. Thus, for $\gamma_m = 2$ the equilibrium density profile across the slab can be directly found and

$$\Theta_\Phi = 4/\pi \approx 1.3.$$

The actual distribution of DM component across a slab and the value of Θ_Φ depends upon the relaxation process which is essentially accelerated by the process of pancake disruption into the system of high density clouds and filaments. In the course of relaxation $\sim 10 - 15\%$ of matter is evaporated what decreases the factor Θ_Φ . This means that the expected $\Theta_\Phi \sim 1$ randomly varies from absorber to absorber.

The Doppler parameter is defined by the depth of potential well (35) and for the isentropic gas with $p_{gas} \propto \rho_{gas}^{5/3}$ trapped within the well, we get

$$b^2 \approx b_{bg}^2 + \frac{4}{5} \Delta\Phi \approx b_{bg}^2 + \frac{3}{10} v_0^2 \frac{q^2}{\delta_m} (1+z) \Theta_\Phi. \quad (36)$$

Variations of the gas entropy across absorbers increase the random variations of $\Delta\Phi$ & b .

For hot absorbers with $b \gg \langle b_{bg} \rangle$ we can neglect the difference between the actual and mean background temperature and in (36) use $\langle b_{bg} \rangle$ instead of b_{bg} . In such a way we link q^2/δ_m with b & $\langle b_{bg} \rangle$ with a reasonable precision.

3.5 Absorbers within rapidly expanded regions

For significant fraction of absorbers – up to 20% – the Doppler parameter is smaller than the expected mean background one (3). Such absorbers are often related to unrecognized metal lines. However, both theoretical arguments and numerical simulations show that such absorbers can also be related to hydrogen clouds formed within colder rapidly expanded regions.

The temperature of relaxed HI absorbers formed by the compression of matter (36) cannot be smaller than the background one (3). However, within low density rapidly expanded regions the background temperature given by (5) is smaller than the mean one, and in such regions the hydrogen clouds with $b_{bg} \leq b \leq \langle b_{bg} \rangle$ can be formed. Our analysis (Sec. 4.5) shows that majority of colder absorbers could be related to such hydrogen clouds.

According to the Zel'dovich theory of gravitational instability and for Gaussian initial perturbations, regions with moderate distortions of the cosmological expansion dominate and probability to find rapidly expanded or compressed regions is exponentially small. However, the observations of galaxies at redshifts under consideration corroborate the existence of strong distortions of cosmological expansion at least on galactic scales. This means that owing to the symmetry of positive and negative initial density perturbations we should also observe rapidly expanded regions with small background density and temperature. Number of such regions exponentially decreases for larger distortions of the expansion.

Owing to the same symmetry, for majority of absorbers, fraction of absorbers with a moderate random expansion and compression in the transverse directions are close to each other and the influence of this factor weakly distorts the mean absorbers characteristics. However, within rapidly expanded regions *all* absorbers are adiabatically expanded in the transverse directions what, in particular, decreases the fraction of neutral hydrogen,

$$x_H \propto n_b/b^{3/2} \Gamma_{12} \propto n_b^{1/2} / \Gamma_{12},$$

and its observed column density, and leads to a systematic drift of absorbers under the observational limit $lg N_{HI} \sim 12$.

Theoretical estimates show that owing to the correlation of velocity perturbations across the pancake and in the transverse directions the rate of pancakes formation within rapidly expanded regions is smaller than the mean one. For the CDM like initial power spectrum the coefficient of correlation of orthogonal velocities is $c_v \approx 1/3$ (DD04). In this case, for the fraction of matter, f_{rap} , and the mean column density of DM component, q_{rap} in the rapidly expanded regions, we expect

$$f_{rap} \approx 0.33 \langle f_{abs} \rangle, \quad \langle \zeta_{rap} \rangle = \langle \zeta(q_{rap}, z) \rangle \approx 0.5 \langle \zeta \rangle. \quad (37)$$

3.6 Characteristics of the gaseous component

The observed column density of the neutral hydrogen can be written as an integral over the line of sight through a pancake

$$N_{HI} = \int dx \rho_b x_H = 2 \langle x_H \rangle \frac{\langle n_b(z) \rangle l_v q}{1+z} \frac{0.5}{\cos\theta}. \quad (38)$$

Here $\langle x_H \rangle$ is the mean fraction of the neutral hydrogen and $\cos\theta$ takes into account the random orientation of absorbers and the line of sight ($\langle \cos\theta \rangle \approx 0.5$). As was noted in Sec. 3.4, we assume also that both DM and gaseous components are compressed together and, so, the column densities of baryons and DM component are proportional to each other.

Under the assumption of ionization equilibrium of the gas (6) and neglecting a possible contribution of macroscopic motions to the b -parameter ($T \propto b^2$), for the fraction of neutral hydrogen and its column density we get:

$$\langle x_H \rangle = x_0 \delta_b \beta^{-3/2} (1+z)^{33/14} \Theta_x, \quad \beta = b / \langle b_{bg} \rangle,$$

$$\frac{N_{HI}}{N_0} = \frac{q \delta_b}{\Gamma_{12} \beta^{3/2}} (1+z)^{61/14}, \quad N_0 = 5.5 \cdot 10^{12} \text{ cm}^{-2} \Theta_H, \quad (39)$$

$$\Theta_H = \frac{\Theta_x}{\Theta_{bg}^{3/7}} \frac{0.15}{\Omega_m h^2} \frac{\langle \cos\theta \rangle}{\cos\theta} \left(\frac{\Omega_b h^2}{0.02} \right)^2, \quad \delta_b = n_b / \langle n_b \rangle,$$

where Γ_{12} , $\langle b_{bg} \rangle$, Θ_{bg} and x_0 were defined in (3) and (7) and the factor $\Theta_x \sim 1$ describes the inhomogeneous distribution of ionized hydrogen along the line of sight.

However, the overdensity of the baryonic component, δ_b is not identical to the overdensity of DM component, δ_m , (see, e.g., discussion in Matarrese & Mohayaee 2002). Indeed, the gas temperature and the Doppler parameter are mainly determined by the characteristics of DM component (36) but the gas overdensity is smaller than that of DM component due to larger entropy of the gas. Moreover, the bulk heating and cooling change the density and entropy of the gas trapped within the DM potential well. These processes change the baryonic density of pancakes and we can write

$$\delta_b = \Theta_b(z) \delta_m, \quad \Theta_b(z) \leq 1. \quad (40)$$

The factor Θ_b should be small for absorbers formed due to adiabatic and weak shock compression because of the large difference between entropies of the background DM and the gas, and $\Theta_b \rightarrow 1$ for richer hot absorbers formed due to strong shock compression when entropies of both components are comparable.

Similarly to the proper thickness of a DM pancake (26),

the thickness of a gaseous pancake is estimated as

$$d_{abs} = \frac{l_v q}{(1+z) \delta_b}. \quad (41)$$

For adiabatically compressed absorbers it is larger than the thickness of the DM pancake but for shock compressed absorbers they are close to each other. So defined d_{abs} can be compared with the estimated redshift thickness of absorbers determined by the observed Doppler parameter,

$$d_v = 2b/H(z). \quad (42)$$

We can expect that, as usual, $d_v \geq d_{abs}$ owing to the impact of thermal velocities. In spite of the limited precision of determination of d_v & d_{abs} these estimates allow us to correct the derived DM column density, q .

For long lived absorbers the influence of the bulk heating can be estimated in the same manner as it was done for characteristics of the background (Demiański & Doroshkevich 2004b). Solving the equation of thermal balance for absorbers formed at $z = z_f$ and observed at $z \ll z_f$ we obtain for the entropy of compressed gas:

$$F_s^{3/2}(z) \approx F_s^{3/2}(z_f) + \frac{8 F_{bg}^{3/2}(z)}{7 \beta^{1/2}(z)} \left[1 - \left(\frac{1+z}{1+z_f} \right)^{3/2} \right]. \quad (43)$$

As is seen from this relation, the bulk heating is negligible for shock compressed absorbers with $F_s(z_f) \gg F_{bg}(z)$, $\beta(z) \gg 1$. For adiabatically compressed long lived absorbers with $z_f \gg z$, $F_s(z_f) \approx F_{bg}(z_f) \leq F_{bg}(z)$ we get

$$F_s^{3/2}(z) \approx F_{bg}^{3/2}(z) / \beta^{1/2}(z), \quad \delta_b \approx \beta^{7/2}. \quad (44)$$

This result demonstrates that the bulk heating is specially important for absorbers with $\beta \ll 1$ formed within rapidly expanded regions. For such absorbers the merging is suppressed and their number decreases mainly owing to the drift under the observational limit.

3.7 Observed characteristics of absorbers

Eqs. (36) and (39) relate three independent variables, namely, q , δ_m & δ_b . To find the DM column density, q , it is therefore necessary to use an additional relation which connects the basic parameters of absorbers. Here we assume that the richer absorbers with $b \geq b_{thr} = \beta_{thr} \langle b_{bg} \rangle > \langle b_{bg} \rangle$ are formed due to shock compression and this process is accompanied by strong relaxation of compressed matter. For such absorbers $\delta_b \approx \delta_m$ and their DM column density is:

$$\delta_b \approx \delta_m \approx \frac{v_0^2 (1+z)}{b^2 - \langle b_{bg} \rangle^2} q^2, \quad b \geq b_{thr},$$

$$q^3 \approx \frac{N_{HI} \Gamma_{12}}{N_0} \frac{b^2 - \langle b_{bg} \rangle^2}{v_0^2} \left(\frac{b}{\langle b_{bg} \rangle} \right)^{3/2} (1+z)^{-75/14}. \quad (45)$$

Formation of absorbers with $b \leq b_{thr} = \beta_{thr} \langle b_{bg} \rangle$ is accompanied by adiabatic or weak shock compression of baryonic component. Assuming that the compression of baryons is described by the polytropic equation of state with $\gamma_b = 5/3$, we can expect that for recently formed absorbers with $b \leq b_{thr}$, $F_s(z) \approx \langle F_{bg}(z) \rangle$,

$$q \approx \frac{N_{HI} \Gamma_{12}}{N_0} \beta^{-3/2} (1+z)^{-61/14}, \quad \delta_b \approx \beta^3, \quad (46)$$

and for long lived absorbers (44)

$$q \approx \frac{N_{HI}\Gamma_{12}}{N_0}\beta^{-2}(1+z)^{-61/14}, \quad \delta_b \approx \beta^{7/2}. \quad (47)$$

The relations (45) – (47) determine the dimensionless column density of DM component corrected for the impact of gaseous pressure. These relations can be successfully applied to absorbers formed due to adiabatic and strong shock compression with various degrees of relaxation. However, the boundary between these limiting cases must be established *a priori*. So, to discriminate absorbers described by (45) and (46, 47), we use the threshold Doppler parameter, b_{thr} which, in fact, characterizes the Mach number of the inflowing matter. Thus, absorbers with $b \leq b_{thr}$,

$$b_{thr} = \beta_{thr}\langle b_{bg}(z) \rangle, \quad \beta_{thr} \approx 1.5 - 2, \quad (48)$$

can be conveniently considered as the adiabatically compressed while absorbers with $b \geq b_{thr}$ are considered as formed by shock compression and they contain strongly relaxed matter.

The precision of these estimates is moderate and the some uncertainties are generated by the poorly known Γ_γ and the parameters Θ_Φ and Θ_H , which vary – randomly and systematically – from absorber to absorber. Estimates of these uncertainties can be obtained from the analysis of the derived absorbers' characteristics. However, the main uncertainties in the estimates of q come from the unknown $\cos\theta$, and, for strongly relaxed shock compressed absorbers, from modulations of b_{bg} .

Indeed, for adiabatically compressed absorbers $q \propto \cos\theta$ and Eqs.(46, 47) underestimate q for $\cos\theta \geq \langle \cos\theta \rangle = 0.5$ and overestimate it for $\cos\theta \leq \langle \cos\theta \rangle$. To reveal and to correct the most serious uncertainties we will use the condition $d_{abs}/d_v \leq 1$ where the real, d_{abs} , and the redshift, d_v , size of absorbers were introduced in (41, 42). For absorbers with $d_{abs} \geq d_v$ we will substitute the 'true' column density, q_t defined by relation

$$q_t = q d_v/d_{abs}, \quad d_{abs} \approx d_v, \quad (49)$$

instead of the measured one (46) or (47). Perhaps, more detailed reconstruction of the shape of absorption lines could allow us to reveal stronger deviations from the Doppler profile and, so, to identify the influence of absorbers orientation and macroscopic velocities.

For shock compressed absorbers the influence of $\cos\theta$ is not so strong as $q \propto \cos^{1/3}\theta$ and the expected modulation of b_{bg} is more important. Indeed, these absorbers are formed owing to the merging which is more probable in slowly expanded regions with $b_{bg} \geq \langle b_{bg} \rangle$. Thus, for absorbers with $b \geq b_{thr}$, $d_{abs} \geq d_v$, we will also correct q & d_{abs} by relation (49).

These corrections essentially improve estimates of the correlation function of initial velocity field.

3.8 Regular and random variations of absorbers' characteristics

The most fundamental characteristic of absorbers is their DM column density, $\zeta(q, z) \propto q(1+z)^2$ (21). It depends on the process of formation and merging of pancakes, is only weakly sensitive to the action of random factors and defines the regular redshift variations of absorbers characteristics.

For shock compressed absorbers, the evolutionary history of each pancake and the action of random factors discussed in the previous subsections are integrated in the entropy of the baryonic component,

$$S_b = \ln F_s(z) = S_{bg} + 2/3 \ln(\beta^3/\delta_b). \quad (50)$$

If the structure of a relaxed DM pancake can be described by the polytropic equation of state with the effective power index γ_m then we can introduce also the entropy of DM component, S_m . For probable value $\gamma_m \approx 1.5 - 2$, entropies of DM and baryonic components are quite similar to each other, $S_m \approx S_b$. This means that for the strongly relaxed shock compressed absorbers the evolutionary history is characterized quite well by two functions, ζ and S_b .

For adiabatically compressed absorbers the baryonic entropy is identical to the background one given by (4) while the observed b and N_{HI} depend upon the distribution of the compressed DM component. For such absorbers the PDFs and the random scatter of observed characteristics are defined mainly by variations of the expansion rate and the background density and temperature. These characteristics as well as the entropy and overdensity of compressed DM component, S_m & δ_m , now cannot be derived from observational data with a reasonable reliability. This problem deserves further investigations.

3.9 Reconstruction of the initial power spectrum

The basic relation of Zel'dovich theory of gravitational instability can be suitably written for the difference of coordinates of two particles,

$$\Delta r_i = \frac{l_v \tau(z)}{1+z} [q_i/\tau(z) - \Delta S_i(q)/l_v], \quad i = 1, 2, 3, \quad (51)$$

where r_i are the Euler coordinates of particles, l_v , $\tau(z)$ and q_i were introduced in (17), (18) & (22) and $S_i(q)$ is a random displacement of a particle with respect to its unperturbed position. As is seen from this relation, for pancakes $\Delta S \approx l_v q/\tau(z)$ and, so, some statistical characteristics of ΔS can be obtained by measuring $q/\tau(z)$.

Using the measured redshift, z , and DM column density of absorbers, q , we determine the cumulative PDF of absorbers $W_{obs}[> q/\tau(z)]$ and, for each $q/\tau(z)$, we compute $\langle q \rangle$ and $\sigma_q^2 = \langle q^2 \rangle - \langle q \rangle^2$. For a chosen $W_q(\zeta)$ (25), we solve numerically the equation

$$W_{obs}[< q/\tau(z)] = W_q(\zeta) = \text{erf}^2(\zeta), \quad (52)$$

with respect to $\zeta(q, \tau)$ and, thus, we obtain the function

$$1 - \xi_v(q) = \frac{q^2}{4\tau^2\zeta(q)}. \quad (53)$$

For the most interesting range $q/\tau(z) \ll 1$, $\zeta \ll 1$ we have

$$W_q(\zeta) \approx 4\zeta^2/\pi, \quad 1 - \xi_v \propto q^2/\sqrt{W_q(\zeta)}. \quad (54)$$

The same approach can be applied to the absorbers separation, d_{sep} , and $\zeta_{rd} = \zeta(q_{rd}, z)$, & q_{rd} introduced by (33). In this case instead of (52) and (54) we have

$$W_{obs}[< d_{sep}/l_v\tau(z)] = W_{sep}(< \zeta_{rd}) \approx 1 - 1.778 \exp(-0.634\zeta_{rd})[1 - 0.425 \exp(-0.634\zeta_{rd})], \quad (55)$$

$$1 - \xi_v(q_{rd}) = \frac{q_{rd}^2}{4\tau^2\zeta(q_{rd})},$$

and, for $q_{rd}/\tau(z) \ll 1$, $\zeta_{rd} \ll 1$, we get

$$W_{sep}(\zeta_{rd}) \approx 0.17\zeta_{rd}, \quad 1 - \xi_v \propto q_{rd}^2/W_{sep}.$$

The observed functions $P_{obs}(q)$ and $P_{obs}(d_{sep})$ can be compared with corresponding expectations (25) and (33). The correlation function $\xi_v(q)$ derived from (53) and (55) can be compared with the reference function $\xi_{CDM}(q)$ (20).

4 MODEL DEPENDENT STATISTICAL CHARACTERISTICS OF ABSORBERS

In this Section, evolution of the basic model dependent characteristics of absorbers is discussed in the Λ CDM cosmological model (1), and for the background temperature, T_{bg} , the Doppler parameter, b_{bg} , and the entropy function F_{bg} given by (3) and (4).

4.1 Parameters of the model

The model of absorbers discussed in Sec. 3 includes poorly known random parameters, Θ_{bg} , Θ_Φ & Θ_x , which cannot be estimated *a priori*, this leads to a moderate random scatter of derived absorbers characteristics. Further on we will assume that

$$\Theta_{bg} = \Theta_\Phi = \Theta_x = 1. \quad (56)$$

However, as was discussed in Sec. 3.7, the main sources of uncertainty in (45 – 47) are the random orientation of absorbers with respect to the line of sight, measured by $\cos \theta$ and, for strongly relaxed shock compressed absorbers, random spatial modulation of the expansion rate and the background temperature, $b_{bg} \geq \langle b_{bg} \rangle$. Large distortions of the derived parameters of absorbers can be revealed and partly corrected using the relation (49). However moderate distortions of the same parameters that can not be easily corrected restrict the precision of our approach.

The poorly known radiative ionization rate, Γ_{12} , (8) is also an important source of uncertainty. As was noted in Sec. 2.1, now there are approximate estimates of the UV background produced by the observed QSOs but the expected ionization rate should be corrected for the absorption and reemission of UV radiation by the gas compressed within high density clouds (Haardt & Madau 1996) and for the additional emission of UV radiations by galaxies (at $z \leq 2$) and at $z \geq 3$ by poorly known sources such as Ly- α emitters (Boksenberg, Sargent & Rauch 2003; Giavalisco et al. 2004; Ouchi 2005).

Below we will describe the ionization rate by the expression

$$\Gamma_{12}(z) \approx G_0 \left(\frac{1+z}{4} \right)^{p_\gamma} \exp \left[-\frac{(z-z_\gamma)^2}{2\sigma_\gamma^2} \right], \quad (57)$$

$$G_0 = 4.3, \quad z_\gamma = 1.0, \quad \sigma_\gamma = 1.58, \quad p_\gamma = 1.5,$$

where the choice of p_γ , z_γ and σ_γ corrects $\Gamma_{12}(z)$ for the impact of additional sources of radiation.

Relatively small value of $\Gamma_{12}(2) \approx 3$ (57) is close to the observational estimates of Scott et al. (2002) and $\Gamma_{12}(5) \approx 0.2$ is similar to the estimates of Fan et al. (2002,

2004). It shows that at $z \sim 2$ the UV background was probably overestimated in Haardt & Madau (1996) and Demiański & Doroshkevich (2004b). Indeed, relatively small observed $\langle N_{HI} \rangle \approx 10^{13.4} \text{ cm}^{-2}$, with $\lg N_{HI} \leq 15$, and moderate number of lines $N_{line} = 226$ with $\lg N_{HI} \geq 15$ in our sample, shows that the absorption of the UV background by HI cannot be very important. However, stronger absorption by HeII found by Levshakov et al. (2003) can distort the spectrum of the UV background and decrease G_0 and the background temperature, T_{bg} & b_{bg} (3). Below the fit (57) will be tested by comparing the theoretically expected and derived functions, $\xi_v(q)$ and $\xi_v(q_s)$, $\langle \zeta(z) \rangle \approx 0.82$ and $\langle l_v q(z) \rangle \approx 0.44 \langle d_{sep}(z) \rangle$.

For such $\Gamma_{12}(z)$ we get for the Gunn–Peterson optical depth, $\tau_{GP}(z)$,

$$\tau_{GP}(2) \approx 0.045 f_{hom}^2, \quad \tau_{GP}(5) \approx 5 f_{hom}^2, \quad (58)$$

where f_{hom} is the fraction of homogeneously distributed matter. Estimates obtained in Sec. 4.3 show that at $z \leq 4$, $f_{hom} \approx 0.5$. However, at such redshifts τ_{GP} is measured for regions with suppressed lines where larger Γ_{12} can be expected. For large $z \geq 4$ we can take $f_{hom} \sim 1$ with large scatter.

The choice of $\Gamma_{12}(z)$ (57) coincides with

$$\tau_0 \approx 0.19, \quad \sigma_8 \approx 0.9,$$

what agrees quite well with σ_8 derived by Spergel et al. (2003, 2006) and with the independent estimate (10). The final results only weakly depend upon the threshold parameter $b_{thr} \approx (1.5 - 2)b_{bg}$ discriminating between adiabatically and shock compressed absorbers. Here we use $b_{thr} \approx 1.5b_{bg}$.

Such choice of the model parameters allow us to obtain reasonable description of properties of absorbers for the selected sample. Variations of limits used for the sample selection lead to moderate variations of parameters (57).

4.2 Correlation functions of the initial velocity field

4.2.1 Correlation functions derived from absorber separations

Using the method described in Sec. 3.9 and characteristics of separations between absorbers obtained in Sec. 2.2 we can estimate also the correlation function of the initial velocity field, $\xi_v(q_{rd})$. This approach uses only the measured redshifts and, so, the derived function does not depend upon the measured b & N_{HI} and the model of absorbers discussed in Sec. 2. However, the theoretically derived PDFs (33) and (55) become unreliable at small separations and, as was noted in Sec. 2.2, already at redshifts $z \sim 3$ the blending of absorbers becomes essential what distorts the derived function $\xi_v(q_{rd})$.

The observed cumulative PDF, in redshift space, $W_{obs}[q_{rd}/\tau(z)]$, and the reconstructed correlation function $1 - \xi_v(q_{rd})$ (55) are plotted in Fig. 3 for the samples of 19 QSOs (6 251 and 7 411 separations) and 14 QSOs (3 660 separations). For these samples we have, respectively,

$$W_{obs}[\langle q_{rd}/\tau(z) \rangle / W_{sep}(\langle \zeta_{fit} \rangle) \approx 1.07 \pm 0.19, \quad 1.03 \pm 0.2,$$

$$\frac{1 - \xi_v(q_{rd})}{1 - \xi_{fit}(q_{rd})} \approx 0.95 \pm 0.25, \quad 1 \pm 0.2, \quad (59)$$

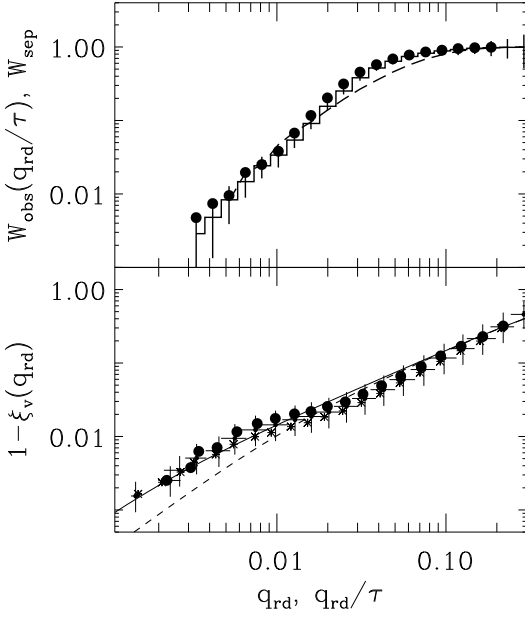


Figure 3. Top panel: the cumulative PDF, $W_{obs}(q_{rd}/\tau)$, together with the fit $W_{sep}(\zeta_{rd})$ (55) (dashed line). Bottom panel: the correlation function of initial velocity field, $1 - \xi_v(q_{rd})$, together with the theoretical fits (20) (dashed line) and the fit (59) (solid line). Points and stars show the same functions found for the sample of 14 QSOs and for the sample of 7411 separations in 19 spectra, respectively.

$$1 - \xi_{fit}(q_{rd}) = \frac{1.5q_{rd}^2}{\sqrt{2.25q_{rd}^4 + q_{rd}^2 + p_s^{1.4}q_{rd}^{0.6}}}, \quad p_s = 2.1 \cdot 10^{-3},$$

$$0.5 \geq q \geq 1.4 \cdot 10^{-3}, \quad 17h^{-1}\text{Mpc} \geq l_v q_{rd} \geq 0.03h^{-1}\text{Mpc}.$$

where $\zeta_{fit} = \zeta(\xi_{fit}, \tau)$ is given by (21).

As is seen from Fig. 3, at $q_{rd} \geq 10^{-2}$, $l_v q_{rd} \geq 0.33h^{-1}\text{Mpc}$ the derived correlation function coincides with the standard CDM – like one (20) for heavy DM particles, with $q_0 \leq 10^{-3}$, $M_{DM} \geq 1\text{MeV}$. Similar results can be found also with the PDF (30) what indicates the weak sensitivity of the derived correlation function ζ_{fit} on the detailed shape of the used PDF.

At small scales, $10^{-3} \leq q_{rd} \leq 10^{-2}$, we see an excess of power with respect to the reference function ξ_v (20). This excess is caused by the deficit of observed absorbers with small separation which increases the derived function, $1 - \xi_v(q_{rd}) \propto W_{sep}^{-1}$ (see Sec. 3.9). In this range of q_{rd} the number of measured separations is limited, $N_{sep} \approx 320$ and $N_{sep} \approx 170$ for the samples of 19 and 14 QSOs, respectively, what decreases reliability of this result. To test impact of this factor we calculated the function $\xi_v(q_{rd})$ for the sample of 7411 separations obtained without placing any restrictions on the properties of absorbers. For this extended sample the number of small separations increases up to 630 but the difference between the derived and reference functions, $\xi_v(q_{rd})$ and $\xi_{CDM}(q_{rd})$, at $q_{rd} \leq 10^{-2}$ remains the same.

These results indicate that possibilities and applicability of this approach are limited. Indeed, the positions of absorbers are measured in the redshift space with a typical error $\Delta z \sim 5 \cdot 10^{-5}$, $\Delta q_{rd} \sim 3 \cdot 10^{-2} [4/(1+z)]^{3/2}$ comparable with the size of absorbers as measured by their Doppler parameter (10), $(1+z)\langle d_v \rangle / l_v \sim 3 \cdot 10^{-2} [4/(1+z)]^{1/2}$. These

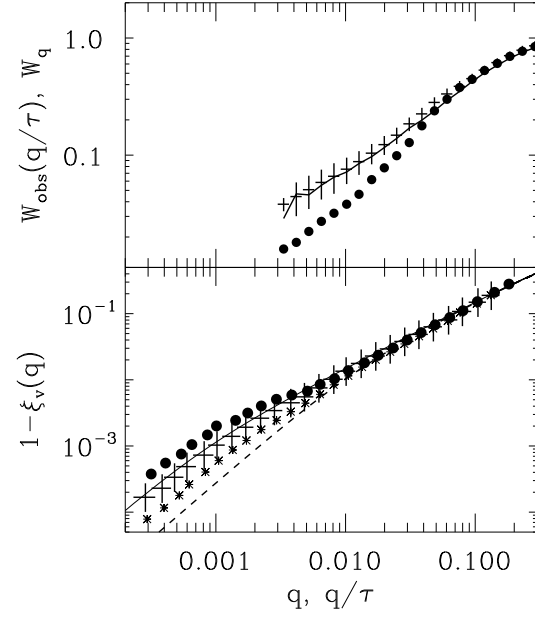


Figure 4. Top panel: the cumulative PDF, $W_{obs}(q/\tau)$, together with fit (52) (long dashed line). Bottom panel: the correlation function of initial velocity field, $1 - \xi_v(q)$, together with the theoretical fit (20) (dashed line) and the fit (60) (solid line). Points and stars show the same functions found for the sample of 14 QSOs and for the sample of 7430 separations.

factors lead to the artificial blending of close absorbers, distort their characteristics and decrease reliability of the estimates (59) for $q_{rd} \leq 10^{-2}$.

4.2.2 Correlation functions derived from DM column density of absorbers

The same correlation function of the initial velocity field, $\xi_v(q)$, can be also found from estimates of the DM column density of absorbers, q . Here we use a more complex procedure of determination of q from the observed z , b , & N_{HI} and poorly known Γ_{12} (57) what decreases its reliability. On the other hand, comparison of the functions ξ_v found with two different approaches allows us to test the model of absorbers discussed in Secs. 3 and 4.1.

The observed cumulative PDF, $W_{obs}(q/\tau)$, and the reconstructed correlation function $1 - \xi_v(q)$ are plotted in Fig. 4 for the samples of 19 QSOs with 6270 and 7430 absorbers and 14 QSOs (3674 absorbers). For these samples we have, respectively,

$$W_{obs}(< q/\tau) / W_q(\zeta_{fit}) \approx 1. \pm 0.07, \quad 0.9 \pm 0.2,$$

$$\frac{1 - \xi_v(q)}{1 - \xi_{fit}(q)} \approx 0.95 \pm 0.15, \quad 1.1 \pm 0.2, \quad (60)$$

$$1 - \xi_{fit}(q) \approx \frac{1.5q^2}{\sqrt{2.25q^4 + q^2 + p_q^{1.4}q^{0.6}}}, \quad p_q = 0.8 \cdot 10^{-3},$$

$$10^{-4} \leq q \leq 0.3, \quad 3h^{-1}\text{kpc} \leq l_v q \leq 9.4h^{-1}\text{Mpc},$$

where $\zeta_{fit} = \zeta(\xi_{fit}, \tau)$ is given by (21).

As is seen from Fig. 4, at $q \leq 5 \cdot 10^{-3}$ the derived correlation function (60) differs from the standard CDM – like one (20). For these q both samples of absorbers are

quite representative with $N_{abs} \approx 1590$ and $N_{abs} \approx 850$ for samples of 19 and 14 QSOs, respectively. However, as was noted above, a more complex procedure of determination of ξ_v decreases its reliability.

At these scales the difference between the derived and reference correlation functions, $\xi_v(q)$ and ξ_{CDM} (20), could be mainly caused by the deficit of weaker absorbers (Sec. 3.9) because $1 - \xi_v(q) \propto W_q^{-1/2}$. As before, to test the impact of this factor we calculated the function $\xi_v(q)$ for the sample of 7430 absorbers with $\lg N_{HI} \leq 15$. For such sample the difference between the derived and reference functions, $\xi_v(q)$ and $\xi_{CDM}(q)$, at $q \leq 10^{-3}$ decreases and the correlation function is fitted by the expression

$$1 - \xi_{fit}(q) = \frac{1.5q^2}{\sqrt{2.25q^4 + q^2 + p_f^{1.4} q_{rd}^{0.6}}}, \quad p_f = 4 \cdot 10^{-3}. \quad (61)$$

The functional forms of expressions (20), (60) and (61) are identical and they differ only by the values of fit parameters $p_q \approx 0.07p_0$, $p_f \approx 0.3p_0$. This means that the difference between ξ_v (60) and ξ_{CDM} (20) could be mainly related to a possible incompleteness of the observed samples of weaker absorbers, to the limited precision of measurements of b & N_{HI} and to the limited precision of our model in describing such absorbers (see discussion in Sec. 3.7).

The correlation function (61) is quite similar to the reference one and their difference is in the range of observational errors. This fact demonstrates that probably the CDM like initial power spectrum can be traced at least down to $q \sim 10^{-4}$, $l_v q \sim 3h^{-1}$ kpc. This means also that $q_0 \leq 10^{-4}$, $m_0 \geq 25$ and the effective mass of the DM particles $M_{DM} \geq 100$ MeV. However, the function (61) is derived from inhomogeneous samples and therefore its reliability is in question.

At larger scales, $q \geq 5 \cdot 10^{-3}$, $l_v q \geq 0.15h^{-1}$ Mpc, results obtained from the analysis of both characteristics of absorbers are quite similar:

$$\frac{1 - \xi_v(q_{rd})}{1 - \xi_{CDM}(q_{rd})} \approx 1.08 \pm 0.25, \quad 1.06 \pm 0.17, \quad (62)$$

$$\frac{1 - \xi_v(q)}{1 - \xi_{CDM}(q)} \approx 1.0 \pm 0.2, \quad 1.09 \pm 0.16. \quad (63)$$

These results confirm the CDM – like type of the initial power spectrum down to scales $l_v q \geq 0.15h^{-1}$ Mpc what extends conclusions of Croft et al. (2002), Viel et al. (2004b); McDonald et al. (2004) and Zaroubi et al. 2005. It also demonstrates the self consistency of the adopted model of absorbers.

It is important, that similar results are found for both samples of 19 QSOs with 6270 absorbers and of 14 QSOs with 3674 absorbers. The samples used are compiled from spectra observed with different instruments and resolutions and the parameters of absorbers were found with different codes what increases their possible non homogeneity. Under these conditions, the stability of our results demonstrates their objectivity.

Reconstruction of the initial power spectrum with the help of the relations (19) shows that in the range of errors the measured and CDM-like power spectra are quite similar each other. At larger k , $k/k_0 \geq 100$, there is some excess of the power but estimates become unstable because of the limited range of measured q . Investigations of this impor-

tant problem should be continued with more homogeneous sample of observed spectra.

4.3 Statistical characteristics of the full sample of absorbers

For the sample of 6270 absorbers the redshift variations of the mean DM column density, $\langle \zeta \rangle$, the mean fraction of DM component accumulated by absorbers, $\langle f_{abs} \rangle$, and the real and redshift sizes of absorbers along the line of sight, $\langle d_{abs} z_4^{3/2} \rangle$, and $\langle d_v z_4^{3/2} \rangle$, are plotted in Fig. 5. The PDFs for the functions ζ and $d_{abs} z_4^{3/2}$ are plotted in Fig. 6. For ~ 1500 absorbers of this sample the parameter q was corrected as described in Sec. 3.7 (Eq. (49)). As was expected, the fraction of such absorbers ($\sim 25\%$) is close to the probability $0 \leq \cos \theta \leq 0.25$ to find absorbers oriented along the line of sight.

The mean DM column density of absorbers, $\langle q \rangle$ or $\langle \zeta \rangle$, is the most stable characteristic of the sample. In principle, $\langle \xi \rangle$ does not change due to the formation and merging of absorbers and due to their transverse compression and/or expansion (DD04). It depends upon the ionization rate, Γ_{12} , the amplitude of initial perturbations, τ_0 or σ_8 , and upon the shape of the correlation function of initial perturbations, ξ_v , or the initial power spectrum, $p(k)$. It also weakly depends upon the parameter b_{thr} used to discriminate absorbers formed by the adiabatic and shock compression. The differences between the expected and measured $\langle \xi \rangle$ characterize, in fact, the completeness and representativity of the samples, the scatter of the function Γ_{12} and the influence of disregarded factors such as Θ_{bg} , Θ_Φ & Θ_x .

For the sample under consideration the redshift variations of the measured $\langle \xi(z) \rangle$ around the mean values are moderate,

$$\langle \zeta \rangle \approx 0.82 \pm 0.08, \quad \langle q z_4^2 \rangle \approx (1.8 \pm 0.2) \cdot 10^{-2}. \quad (64)$$

At small and larger redshifts, $z \leq 2$ and $z \geq 3.7$, limited statistic of absorbers decreases reliability of our estimates. The measured $\langle \zeta(z) \rangle$ is close to the theoretically expected value (25) what verifies the choice of the ionizing rate $\Gamma_{12}(z)$ in (57) and the amplitude of initial perturbations, $\tau_0 = 0.19$, $\sigma_8 \approx 0.9$.

The PDF of the DM column density, $P(\zeta)$ plotted in Fig. 6 is fitted with a scatter $\sim 10\%$ by the function

$$P(x_\zeta) = 1.2 \exp(-x_\zeta) \operatorname{erf}(\sqrt{x_\zeta}) / \sqrt{x_\zeta}, \quad x_\zeta = \zeta(q, z) / \langle \zeta \rangle, \quad (65)$$

which is very close to the theoretical relation (25). This result verifies the self consistency of the physical model used here and the assumed Gaussianity of initial perturbations.

As is well known, for the full sample the HI column density and Doppler parameter are weakly correlated, and for our sample their linear correlation coefficient is

$$R_{bHI} = [\langle b N_{HI}^* \rangle - \langle b \rangle \langle N_{HI}^* \rangle] / \sigma_b \sigma_{HI}^* \approx 0.16, \quad (66)$$

where $N_{HI}^* = N_{HI} / z_4^2$. At the same time, the DM column density, ζ , is correlated with both the HI column density and Doppler parameter, and the linear correlation coefficients defined in the same manner as (66) are

$$R_{\zeta_b} \approx 0.34, \quad R_{\zeta_{HI}} \approx 0.72. \quad (67)$$

The PDF of observed absorber separations, $P(x_{rd})$,

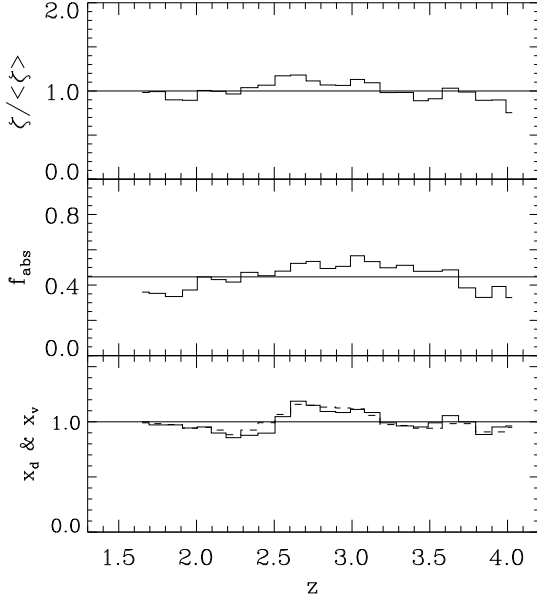


Figure 5. Functions $\zeta(z)/\langle\zeta\rangle$, (top panel), the matter fraction accumulated by absorbers, $f_{abs}(z)$, (middle panels), and the real and redshift sizes of absorbers, x_d (70), and $x_v = d_v(z)z_4^{3/2}/\langle d_v z_4^{3/2}\rangle$, (bottom panel, solid and dashed lines).

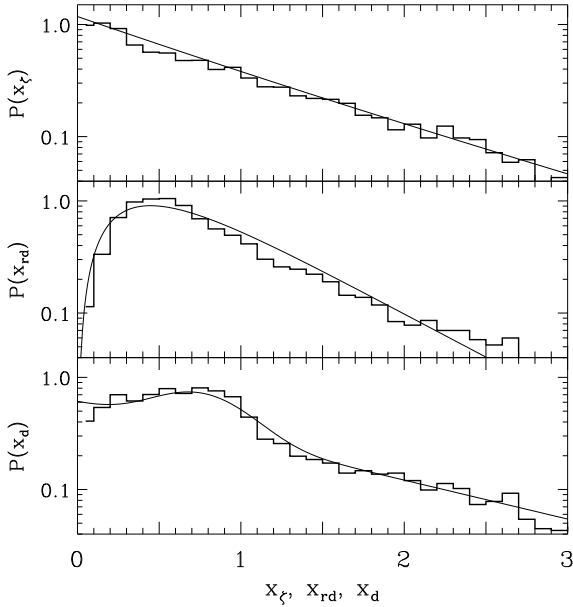


Figure 6. PDF for the DM column density, $P(x_\zeta)$, (top panel), the absorber separation, $P(x_{rd})$, (middle panel), and for the absorber thickness, $P(x_d)$ (bottom panel) are plotted together with fits (65), (68) and (70).

plotted in Fig. 6 is fitted with a scatter $\sim 13\%$ by the function

$$P(x_{rd}) = 3.56 \exp(-1.6x_{rd}) \text{erf}^4(\sqrt{1.6x_{rd}}/\sqrt{x_{rd}}), \quad (68)$$

where $x_{rd} = \zeta_{rd}(d_{sep}, z)/\langle\zeta_{rd}\rangle$, $\langle\zeta_{rd}\rangle \approx 1.5$ and $\zeta_{rd}(d_{sep}, z)$ was introduced in (33). At small and large x_{rd} this fit differs from the theoretically expected one for redshift space (33) but it is quite similar to the fit (30) for the PDF of separa-

tions in Lagrangian space. Perhaps, this fact can be related to the unexpectedly moderate influence of the peculiar velocities of absorbers. However, it can be partly caused by peculiarities of our samples.

Our model of absorbers (see Sec. 3) allows one to estimate roughly the real size of baryonic distribution across the absorber, d_{abs} , (41). For the full sample we have

$$\langle d_{abs}^* \rangle = \langle d_{abs} z_4^{3/2} \rangle \approx (0.11 \pm 0.01) h^{-1} \text{Mpc}, \quad (69)$$

$$\langle d_v^* \rangle = \langle d_v z_4^{3/2} \rangle \approx (0.12 \pm 0.01) h^{-1} \text{Mpc},$$

and both sizes increase with time. The PDF of the real size of baryonic pancakes is roughly fitted by:

$$P(x_d) \approx 0.6 \exp(-0.8x_d) + 0.4 \exp[-(0.73 - x_d)^2/0.15], \quad (70)$$

$$x_d = d_{abs}^* / \langle d_{abs}^* \rangle = d_{abs} z_4^{3/2} / \langle d_{abs} z_4^{3/2} \rangle,$$

with a scatter $\sim 12\%$.

For the expected mean transverse size of absorbers (27) and for model parameters (57) we have for the mean proper size

$$\langle l_v q_{tr} \rangle (1+z)^{-1} \approx 0.45 z_4^{-2} (1+z)^{-1} h^{-1} \text{Mpc},$$

what is consistent with recent direct estimates by Becker, Sargent & Rauch (2004) at $z \sim 3 - 3.5$

$$l_v q_{tr} \approx (0.15 - 0.2) h^{-1} \text{Mpc}.$$

The exponential PDF of the transverse sizes (27) and its strong redshift dependence explain large scatter of the sizes ($l_v q_{tr} \leq 1 h^{-1} \text{Mpc}$) measured in many observations of pairs of QSOs (see, e.g., discussion in Becker, Sargent & Rauch 2004).

The mean measured fraction of matter accumulated by absorbers is

$$\langle f_{abs}(z) \rangle \approx 0.44 \pm 0.07. \quad (71)$$

In spite of the limited applicability of the one dimensional approach (31) and the limited precision of our model of absorbers the measured fraction (71) is close to the theoretical expectation of the Zel'dovich theory (32) what verifies the choice of the model characteristics (Sec. 4.1). The weak redshift variations of this function agrees well with the self similar evolution of absorbers.

4.4 Adiabatically and shock compressed absorbers

To investigate the complicated evolution of absorbers in more details, we compare subpopulations of adiabatically and shock compressed absorbers. These subpopulations were separated by comparison of the measured Doppler parameter, b , with the background one $\langle b_{bg} \rangle$, (3). By definition, absorbers with $b \geq b_{thr} = 1.5 \langle b_{bg} \rangle$ belong to the subpopulation of shock compressed and strongly relaxed absorbers, while absorbers with $b \leq b_{thr} = 1.5 \langle b_{bg} \rangle$ are considered as formed in a course of adiabatic or weak shock compression. This discrimination is not strict however and characteristics of subpopulations depend upon the sample used in the analysis and the parameters of the parameters of the background (3, 57). This classification allows one to characterize reasonably well the observed absorbers and to trace their evolutionary history. For both subpopulations, redshift variations of the mean characteristics are listed in Table 2 and some of the PDFs are plotted in Fig.7.

Table 2. Mean parameters of adiabatically and shock compressed absorbers

	adiabatic	shock
$\langle \lg N_{HI}/z_4^2 \rangle$	13.2 ± 0.07	13.5 ± 0.1
$\langle b \rangle \text{ km/s}$	21 ± 0.9	48 ± 5
$\langle f_n \rangle$	0.8 ± 0.06	0.2 ± 0.05
$\langle f_{abs} \rangle$	0.33 ± 0.05	0.11 ± 0.08
$\langle \zeta \rangle$	0.77 ± 0.07	1.1 ± 0.2
R_{ζ_b}	0.39	0.42
$R_{\zeta_{HI}}$	0.75	0.77
$\langle \delta_b \rangle$	$\beta^{7/2}$	$(2 \pm 0.3)z_4^{-2.5}$
$\langle S_b + 2 \ln z_4 \rangle$		2.3 ± 0.2
$\langle d_{abs} z_4^{3/2} \rangle h^{-1} \text{ Mpc}$	0.09 ± 0.01	0.18 ± 0.05
$\langle d_v z_4^{3/2} \rangle h^{-1} \text{ Mpc}$	0.1 ± 0.05	0.22 ± 0.02

$z_4 = (1+z)/4$, f_n and f_{abs} are the fraction of absorbers and of matter in absorbers, R_{ζ_b} & $R_{\zeta_{HI}}$ are the linear correlation coefficients of hydrogen and DM column densities and Doppler parameter defined in the same manner as (66), δ_b and S_b are the overdensity above the mean density and relative entropy of compressed baryonic component, d_{abs} and d_v are the real and redshift sizes of absorbers along the line of sight.

For the sample under investigation $\sim 80\%$ of absorbers are compressed adiabatically and they accumulate $\sim 80\%$ of the compressed matter. These fractions, f_n & f_{abs} , weakly vary with redshift. The PDFs, $P(x_\zeta)$, $x_\zeta = \zeta/\langle \zeta \rangle$, plotted in Fig. 7 for both subpopulations are quite similar to each other and to the PDFs (34) and $P(x_\zeta)$ (65) plotted in Fig. 6 for the full sample. It demonstrates that in wide range of redshifts absorbers could be formed by both processes while the cutoff at $\zeta = 0.3\langle \zeta \rangle$ in the PDF for shock compressed absorbers is imposed by the method used for the discrimination of absorbers. For both samples, the correlation coefficients R_{ζ_b} and $R_{\zeta_{HI}}$ defined in the same manner as (66) are similar to each other. These similarities verify the generic nature of absorbers and indicate that they can be successfully combined into one sample, what is consistent with expectations of the Zel'dovich theory. For the subpopulation of shock compressed and strongly relaxed absorbers $\langle \zeta \rangle \approx \langle \zeta_{mrg} \rangle$ (34), as expected for merged absorbers, what confirms the importance of merging in the process of absorbers' evolution.

For both subpopulations $\langle b/b_{inf} \rangle \leq 1$, what can be partly related to evaporation of high velocity particles in the course of relaxation of the compressed matter. For both subpopulations, the redshift size of absorbers along the line of sight, d_v , is larger than the real size, d_{abs} (Table 2). The redshift dependence $d_{abs} \propto z^{-3/2}$ is consistent with the evolution of their redshift size. The PDFs of the real size of absorbers, $P(x_d)$, is plotted in Fig. 7.

For adiabatically compressed absorbers the entropy is the same as for the background while the overdensity, $\delta_b = \beta^3$, is determined by b and b_{bg} . In particular, for cold absorbers with $b \leq b_{bg}$ we have $\delta_b \leq 1$.

For subpopulation of strongly relaxed and shock compressed absorbers both the entropy and the overdensity depend upon the complex evolutionary history of absorbers and cannot be described by a simple theoretical model. For such absorbers growth of the overdensity with time can be explained by the action of several factors such as successive merging and contribution of long lived absorbers formed at

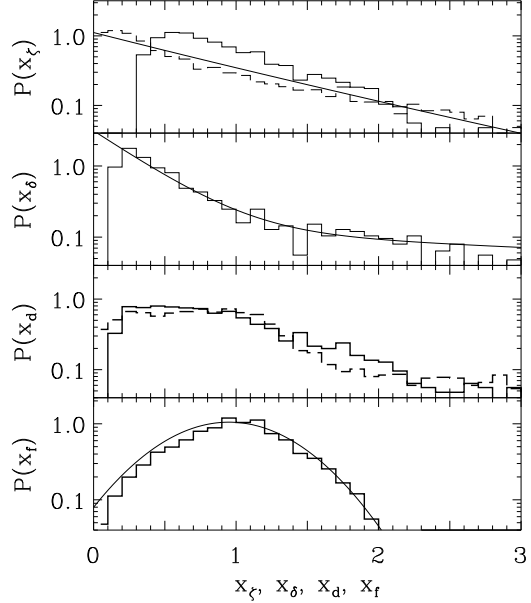


Figure 7. The PDFs for the DM column density, $P(x_\zeta)$, overdensity, $P(x_\delta)$, and the real size across the absorber, $P(x_d)$, (three top panels) are plotted for shock compressed (solid lines) and adiabatically compressed (dashed lines) absorbers together with fits (65) and (72). For shock compressed absorbers, the PDFs for the baryonic entropy, $P(x_f)$, is plotted in bottom panel with fit (73).

redshifts z_f larger than the observed one, $z_{obs} \leq z_f$. For such absorbers the measured PDF $P(x_\delta)$ is plotted in Fig. 7 and it can be fitted by a superposition of two exponential functions:

$$P(x_\delta) \approx 3 \exp(-3.1x_\delta) + 0.13 \exp(-0.2x_\delta), \quad (72)$$

$$x_\delta = \delta_b(1+z)^{2.5} / \langle \delta_b(1+z)^{2.5} \rangle.$$

The entropy of strongly relaxed and shock compressed baryons (50) increases with time and its PDF plotted in Fig. 7 is well fitted by the Gauss function

$$P(x_f) \approx \exp[-(x_f - 0.95)^2 / 0.35], \quad (73)$$

$$x_f = \ln[F_s(z)z_4^2] / \langle \ln[F_s(z)z_4^2] \rangle.$$

Such PDF naturally arises when the entropy is generated by the action of many random factors such as the shock waves accompanying the successive merging of absorbers.

4.5 Absorbers in rapidly and moderately expanded regions

As was discussed in Sec. 3.5, we expect that majority of absorbers with small Doppler parameters, $b \leq b_{rap} \approx 23.5$ km/s, and especially with $b \leq \langle b_{bg} \rangle$ could be formed within rapidly expanded regions and, so, they can characterize some properties of these regions. Some characteristics of absorbers with $b \leq b_{rap}$ are listed in Table 3 in comparison with the same characteristics of adiabatically compressed absorbers with $b_{thr} \geq b \geq b_{rap}$ situated within moderately expanded regions.

The rapidly expanded regions accumulate $\langle f_n \rangle \sim 50\%$ of adiabatically compressed absorbers and $\langle f_{rap} \rangle \sim 30\%$ of adiabatically compressed matter. These values practically

Table 3. Parameters of absorbers in rapidly and moderately expanded regions

	rapidly	moderately
$\langle \lg N_{HI}/z_4^2 \rangle$	$13. \pm 0.1$	13.4 ± 0.1
$\langle b \rangle km/s$	15.5 ± 0.6	27 ± 1.2
$\langle f_n \rangle$	0.49 ± 0.05	0.51 ± 0.05
$\langle f_{abs} \rangle$	(0.11 ± 0.05)	(0.22 ± 0.05)
$\langle \zeta \rangle$	0.46 ± 0.04	1 ± 0.1
$R_{\zeta b}$	0.8	0.07
$R_{\zeta HI}$	0.4	0.76
$\langle D_{reg} z_4^2 \rangle h^{-1} \text{Mpc}$	(1.6 ± 0.2)	(3.2 ± 0.4)
$\langle d_{abs} z_4^{3/2} \rangle h^{-1} \text{Mpc}$	(0.08 ± 0.01)	(0.1 ± 0.01)
$\langle d_v z_4^{3/2} \rangle h^{-1} \text{Mpc}$	(0.08 ± 0.003)	(0.12 ± 0.005)

$z_4 = (1+z)/4$, $\langle f_n \rangle$ and $\langle f_{abs} \rangle$ are the fraction absorbers and of matter in absorbers, $R_{\zeta b}$ & $R_{\zeta HI/z_4^2}$ are the linear correlation coefficients of hydrogen and DM column densities and Doppler parameter defined in the same manner as (66), $\langle D_{reg} \rangle$ is the mean size of rapidly and slowly expanded regions, $\langle d_{sep} \rangle$ and $\langle d_v \rangle$ are the mean absorber separation and their mean redshift size along the line of sight,

do not depend on the redshift. The Doppler parameter, b , and the DM column density, $\zeta_{rap}(q, z)$, also weakly depend upon redshift. For this subpopulation we have

$$\langle \zeta_{rap} \rangle \sim 0.5 \langle \zeta \rangle, \quad \langle f_{rap} \rangle \sim 0.25 \langle f_{abs} \rangle. \quad (74)$$

As was noted in Sec. 2.2, the mean size of rapidly expanded regions, $\langle D_{rap} \rangle$, as well as the mean separation of absorbers within these regions, $\langle d_{sep} \rangle$, increase with time in the same manner as the mean separation of absorbers for the full sample (10). At $z_4 \sim 1$ the typical mass associated with rapidly expanded regions, M_{rap} (14), is in the range of galactic masses and it increases with time $\propto (1+z)^{-3}$. This result is consistent with the expected symmetry of positive and negative initial density perturbations what leads to formation of both galaxies and rapidly expanded regions. These results are consistent with theoretically expected ones (37), what confirms the interpretation of the complex shape of PDF $P_b(b)$ and subpopulation of weak absorbers proposed in Sec. 3.5.

For the subpopulation of moderately expanded absorbers variations of the Doppler parameter, b , are small, $R_{\zeta b} \ll 1$ and the DM column density, ζ , depends mainly upon the hydrogen column density, N_{HI} . In contrast, for the rapidly expanded absorbers the influence of both b & N_{HI} are equally important. In spite of this difference, for both subpopulations the PDFs $P(\zeta)$ are quite similar to each other and to the PDF (65) obtained for the full sample. This fact indicates that the interaction of small and large scale perturbations changes $\langle \zeta \rangle$ more strongly but only weakly influences the shape of the PDFs $P(\zeta)$.

For both subpopulations, the mean proper sizes of absorbers, $\langle d_{abs} \rangle$, are similar (Table 3) but their PDFs are quite different. Thus, for rapidly expanded regions the PDF $P(x_d)$ is step-like and it is responsible for the bump at $d_{abs} z_4^{3/2} \leq \langle d_{abs} z_4^{3/2} \rangle$ in the PDF $P(x_d)$ plotted in Fig. 6. This distribution differs from the distribution of Doppler parameter, $P(x_b)$, what suggests a complex internal structure of such absorbers.

4.6 Absorbers and properties of the background

Some characteristics of absorbers could be used to estimate the redshift variations of the mean properties of homogeneously distributed hydrogen (see, e.g., Hui & Gnedin 1997; Schaye et al. 1999, 2000; McDonald et al. 2001). However, such estimates are inevitably approximate and their significant scatter is caused by the action of many random factors discussed above. To obtain more stable results Schaye et al. (1999, 2000) consider a cutoff at small b in the distribution of $b(N_{HI})$. However, such absorbers are probably formed within rapidly expanded regions and for them both background properties and expansion rate vary randomly from absorber to absorber.

For the subpopulation of moderately expanded absorbers, we can combine Eqs. (41), (42), (36) and (46) and, in principle, connect the background temperature with the Doppler parameter of absorbers, b , and their hydrogen column density, N_{HI} . However, reliability and significance of such estimates are in question. Some restrictions on the intensity of UV background were discussed in Sec. 4.1.

5 SUMMARY AND DISCUSSION.

In this paper we continue the analysis initiated in Paper I and Paper II that is based on the statistical description of Zel'dovich pancakes (DD99, DD04). This approach allows one to connect the observed characteristics of absorbers with fundamental properties of the initial perturbations without any smoothing or filtering procedures, to reveal and to illustrate the main tendencies of structure evolution. It demonstrates also the generic origin of absorbers and the Large Scale Structure observed in the spatial distribution of galaxies at small redshifts.

We investigate the more representative sample of ~ 6000 absorbers what allows us to improve the physical model of absorbers introduced in Paper I and Paper II and to obtain reasonable description of physical characteristics of absorbers. The progress achieved demonstrates again the key role of the representativity of the observed samples for the construction of the physical model of absorbers and reveals a close connection between conclusions and the observational database. Further progress can be achieved with richer and more refined sample of observed absorbers.

5.1 Main results

Main results of our analysis can be summarized as follows:

- (i) For suitable parameters of the model (Sec. 4.1), the basic observed properties of absorbers and their evolution are quite successfully described by the statistical model of DM confined structure elements (Zel'dovich pancakes) with various evolutionary histories. Comparison of independent estimates of the DM characteristics of pancakes confirms the self consistency of the physical model. This model is in a good agreement with measured properties of metal systems (see, e.g. Carswell, Schaye & Kim 2002; Telferet al. 2002; Bergeron & Herbert-Fort 2005).
- (ii) The PDFs of the DM column density and the distances between neighboring absorbers are found to be consis-

tent with the Gaussian initial perturbations with the CDM-like initial power spectrum.

(iii) For the observed range of redshifts the evolution of absorbers is close to self-similar one. This implies that it leads to slow variations of mean absorber characteristics with redshift and retains their PDFs.

(iv) We estimate the shape of the correlation function of the initial velocity field what in turn allows us to estimate the shape of the initial power spectrum. At scales $\geq 0.15h^{-1}$ Mpc both derived correlation functions, (59) and (60), reproduce the CDM-like one. This means that at such scales the power spectrum of initial perturbations is close to the standard one (16). At smaller scales we see some differences between the derived and CDM-like correlation functions which depend upon the sample used in the analysis.

(v) Analysis of variations of the Doppler parameter, b , along the line of sight demonstrates existence of rapidly expanded regions which can be considered as examples of strong negative density perturbations of galactic mass scale.

(vi) Our analysis shows that in the observed range of redshifts we can expect slow variations of the intensity of UV background radiation and of the ionization rate, Γ_{12} . Our results are close to the estimates of the UV background in Haardt & Madau (1996), Scott et al. (2002), and Demiański & Doroshkevich (2004b).

5.2 Test of the model of absorbers

The physical model of absorbers introduced in Sec. 3 links the measured z , b and N_{HI} with other physical characteristics of both gaseous and DM components forming the observed absorbers. It is important that this 1D model provides us with the self consistent statistical description of the Ly- α forest although some parameters of pancakes remain unknown. Action of these parameters as well as uncertainties in the available estimates of the background temperature and the UV background radiation lead to moderate random scatter of the derived characteristics of absorbers. Fortunately, actions of these factors partly compensate each other, what allows us to obtain reasonable statistical description for majority of absorbers. The self consistency of this approach is confirmed by similarity of the functions $\xi_v(q_{rd})$ (59) and $\xi_v(q)$ (60) and by estimates of the matter fraction, f_{abs} , accumulated by absorbers (71). These functions are related to independent characteristics of absorbers obtained from measurements of their separation and their DM column density.

For richer absorbers, both the hydrostatic equilibrium of compressed matter along the shorter axis of pancakes and the close link between the gas temperature and the Doppler parameter, b , are confirmed by comparison of characteristics of the HI and metal systems (see, e.g. Carswell, Schaye & Kim 2002; Telferet al. 2002; Simcoe, Sargent & Rauch 2002, 2004; Boksenberg, Sargent and Rauch 2003; Manning 2002, 2003 a,b; Bergeron & Herbert-Fort 2005). In particular, for 191 high resolution metal systems presented in Boksenberg, Sargent and Rough (2003) differences between the gas temperatures measured by the Doppler parameters of HI and CIV do not exceed $\sim 25\%$, what is comparable to the precision of measurements. Comparison of the Doppler parameters measured for HI, CIV and OVI (Carswell, Schaye & Kim 2002) verifies also their similarity and shows that as

a rule the macroscopic (turbulent) velocities are subsonic. These observational results strongly support the domination of long-lived gravitationally bound and partly relaxed absorbers composed of both DM and baryonic components.

Numerical simulations show that the line width depends upon the thermal broadening, the differential Hubble flow and peculiar velocities and the relative influence of these factors varies from absorber to absorber (see, e.g., Theuns, Schaye & Haehnelt 2000; Schaye 2001). The Hubble flow is more essential for weaker absorbers and can artificially increase their Doppler parameter. For majority of absorbers in the considered 1D model the possible contribution of Hubble flow is naturally linked with the compression or expansion of pancakes in the transverse directions and depends upon the (unknown) relative orientation of absorber and the line of sight. The available observational data do not allow to discriminate between the thermal and macroscopic broadening of the lines what increases the random scatter of our results. To perform such discrimination a more detailed description of the observed line profiles is required.

One of the important problem facing the high resolution numerical simulations is the development of the methods for the more detailed reconstruction of the physical properties and revealing of links between the DM and baryonic components of observed absorbers. In particular, this includes the discrimination of the thermal and macroscopic broadening of lines, explanation of the surprisingly weak redshift dependence of the mean Doppler parameter, detection of the complex internal structure of absorbers as indicated by the observations of metal systems and so on.

However, now technical limitations restrict facilities of simulations. Thus, the small box size used eliminates the large scale part of the power spectrum and decreases the representativity of simulated sample of absorbers. As was discussed in Paper II and in Manning (2003 a,b), these factors eliminate the interaction of large and small scale perturbations and distort characteristics of the simulated absorbers. Simulations reproduce the observed transmitted flux and its main features and now they are used mainly for the surprisingly stable reconstruction of the initial power spectrum from the flux characteristics (see, e.g., Seljak et al. 2004; McDonald et al. 2004, Viel et al 2004a, b). However, the analysis of Meiksin, Bryan and Machacek (2001) shows that simulations have problems with reproduction of the observed PDFs for the column density of neutral hydrogen, N_{HI} , and the Doppler parameter, b , and their self similar redshift evolution.

More detailed criticism of the ‘‘Fluctuating Gunn-Petersen approximation’’ and the simulations of the forest can be found in Manning (2002, 2003 a,b), Paper II and references cited in these papers.

5.3 Properties of absorbers

Analysis of the mean absorbers characteristics performed in Sec. 4 shows that the sample of observed absorbers is composed of pancakes with various evolutionary histories. We discuss five main factors that determine evolution of absorbers after their formation. They are: the transverse expansion and compression of pancakes, the disruption of structure elements into a system of high density clouds, the merging of absorbers and the radiative heating and cooling

of compressed gas. The first two factors change the overdensity of DM and gas but do not change the gas entropy. Next two factors change both the gas entropy and overdensity but do not change the DM characteristics.

The sample of observed forest can be naturally divided into subsamples of adiabatically and shock compressed absorbers formed by merging. Moreover, about half of adiabatically compressed absorbers are formed within rapidly expanded regions where the background temperature is less than mean one. So, the temperature of absorbers formed within such regions can be also less than the mean temperature of the background (3). These results illustrate the influence of some of the factors mentioned above. However, the slow variation of the mean characteristics of absorbers and their PDFs with redshift confirms that we observe the self-similar period of absorbers evolution when the action of these factors is balanced and regular variations of the UV background does not distort this balance.

For shock compressed absorbers, introduction of the DM column density, q and ζ , and entropy, $S_m \approx S_b$, allows to discriminate between the systematic and random variations of their properties. The former ones are naturally related to the progressive growth with time of the DM column density of absorbers, $q(z)$ & $\zeta(z)$, and they can be described theoretically. On the other hand the action of random factors cannot be satisfactorily described by any theoretical model. However, in the framework of our approach, the joint action of all random factors is summarized by one random function, S_b , directly expressed through the observed parameters (50). These results alleviate the problem of description of absorbers and, perhaps, the modelling of the Ly- α forest based on the simulated DM distribution (Viel et al. 2002).

For adiabatically compressed absorbers, the spatial distributions, entropy and overdensity of baryonic and DM components are different. Unfortunately at present these characteristics of DM component cannot be determined from observations with a reasonable accuracy. For such absorbers the baryonic entropy is identical to the background one given by (4) while the PDFs and the random scatter of observed characteristics are determined mainly by random variations of the expansion rate and the background density and temperature. For this subpopulation, the process of formation and evolution of absorbers should be investigated more thoroughly.

5.4 Characteristics of the initial power spectrum

The initial power spectrum of density perturbations is created at the period of inflation and its observed determination is very important for investigations of the early Universe. The amplitude and the shape of large scale initial power spectrum are approximately established by investigations of relic radiation (see. e.g. Spergel et al. 2003, 2006) and the structure of the Universe at $z < 1$ detected in large redshift surveys such as the SDSS (Dodelson et al. 2002; Tegmark et al. 2004) and 2dF (Percival et al. 2001). The shape of the initial power spectrum at small scale can be tested at high redshifts where it is not so strongly distorted by non-linear evolution (see, e.g., Croft et al. 2002; Tegmark et al. 2002; McDonald et al. 2004; Seljak et al. 2004; Zaroubi et al. 2005).

Here we retrieve the correlation function of initial ve-

locity field, ξ_v , from direct measurements of the PDFs of fundamental characteristics of absorbers such as their separation, d_{sep} , and the DM column density, q . Both estimates are derived in the same way and result in the same shape of the correlation function at larger scales, $q \geq 5 \cdot 10^{-3}$, $l_v q \geq 0.15 h^{-1}$ Mpc. At these scales the measured correlation functions coincide with the CDM-like one (20) what confirms conclusions of Croft et al. (2002), Viel et al. (2004b); McDonald et al. (2004) and Zaroubi et al. (2005) obtained at scales $\geq 1 h^{-1}$ Mpc.

At smaller scales the results obtained with analysis of the absorbers separation, d_{sep} , and the DM column density, q , are different and demonstrate some excess of power at scales $150 \text{ kpc} \geq l_v q \geq 3 \text{ kpc}$. Parameters of these functions and the excess depend upon the sample of absorbers and for the extended samples the derived correlation functions become quite similar to the CDM-like one. However, reliability of this result is in question due to a probable incompleteness of the extended samples.

The interpretation of these distortions is not unique because of very limited available information. As was shown in Sec. 4.2, they are sensitive to the deficit of weaker absorbers and small separations of absorbers in the sample under consideration. Therefore these distortions can be enhanced by the probable incompleteness of the observed sample created by the finite resolution of observations, blending of lines and approximate character of our analysis. If this explanation is correct than these factors restrict the presently available range of investigations to $l_v q \geq 100 \text{ kpc}$. Further progress can be achieved with more refined observations of absorption spectra of QSOs and with more refined identification of absorbers in the observed spectra.

In turn, these divergences can be related to special features in the initial power spectrum at small scales. Recent WMAP measurements indicate that adiabatic Gaussian perturbations dominate on large scale (Peiris et al. 2003; Komatsu et al. 2003). However, these results do not preclude deviations from the standard CDM-like power spectrum at small scales. In particular, such deviations appear in models of the one field inflation with a complicated inflation potential (see, e.g., Ivanov, Naselsky & Novikov 1994) or multiple fields inflation (see, e.g., Polarski & Starobinsky 1995; Turok 1996). Both models generate adiabatic or isocurvature deviations from the simple CDM-like power spectrum. More detailed discussion of such models can be found, for example, in Peiris et al. (2003).

5.5 Absorbers as elements of the Large Scale Structure of the Universe

At redshifts $z \geq 1.7$ the Large Scale Structure is observed mainly as systems of absorbers in spectra of distant QSOs. Numerical simulations show that even at such redshifts we can see also high density filaments and clumps formed by “galaxies” and some of them are actually observed in spectra of QSOs as metal systems, Lyman damped and Lyman limit systems. However, available observational data do not yet allow one to characterize statistically properties of such structure elements (see, e.g., Boksenberg, Sargent & Rauch 2003).

At small redshifts, the Large Scale Structure is observed as a spatial distribution of both galaxies and neutral hydro-

gen. The investigation of galaxy distribution in the SDSS DR1 (Doroshkevich, Tucker, Allam & Way 2004a) results in estimates of typical parameters of galaxy walls as

$$\langle q \rangle \approx 0.4, \quad \langle b \rangle \approx 320 \text{ km/s}, \quad \langle d_{sep} \rangle \approx 60 h^{-1} \text{ Mpc}. \quad (75)$$

With these data the expected column density of neutral hydrogen within the typical wall (38) is $N_{HI} \approx 10^{11} \text{ cm}^{-2}$ and even so spectacular object as the 'Greet Wall' does not manifest itself through absorbers.

Our results indicate the generic link of absorbers and DM Zel'dovich pancakes and demonstrate that the embryos of walls could also be seen already at $z \sim 3$. Indeed, for basic parameters of subpopulation of 1 370 shock compressed absorbers with $b \geq 30 \text{ km/s}$ we have

$$\langle d_{sep} \rangle \approx (50 \pm 11)(1+z)^{-2} h^{-1} \text{ Mpc}, \quad (76)$$

$$\langle q \rangle \approx (0.4 \pm 0.07)(1+z)^{-2},$$

what is quite similar at $z=0$ to that given in (75). This fact indicates that, in principle, such absorbers can be considered as embryos of wall-like elements of the Large Scale Structure of the Universe. Of course, such identification of walls observed in the galaxy distribution with elements of Ly- α forest is quite arbitrary and ignores the actual complex evolution of the LSS elements. However, it confirms generic character of the LSS evolution from richer absorbers to galaxy walls. The problem deserves further investigation first of all with more representative numerical simulations.

For the first time poor absorbers at small redshifts were observed by Morris et al. (1991, 1993) and ~ 1000 of such absorbers were found by Bahcall et al. (1993, 1996) and Januzzi et al. (1998). Some of these absorbers are identified with halos of galaxies (see, e.g., Lanzetta et al. 1995; Le Brune, Bergeron & Boisse 1996) or galaxy filaments (Penton, Shull & Stock 2002) but others are situated far from any galaxies. These observations demonstrate that the space between the LSS elements – so called 'voids' – is not empty and contains essential fraction of baryonic and DM components of the matter.

More detailed characteristics of absorbers at $z \ll 1$ are given in Penton, Shull & Stock (2000, 2002); McLin et al. (2002) where the main absorber properties are found to be similar to those observed at high redshifts. For 79 absorbers with $12 \leq \lg N_{HI} \leq 15$, $11 \text{ km/s} \leq b \leq 80 \text{ km/s}$ listed in these papers the mean absorber separation is

$$\langle d_{sep} \rangle \sim (10 \pm 3) h^{-1} \text{ Mpc}. \quad (77)$$

Despite the strong difference of many conditions at $z \ll 1$ and $z \geq 1.5$, these observed characteristics of absorbers are quite similar to expected ones (10) extrapolated to $z = 0$.

5.6 Observed and expected evolution of the Large Scale Structure

Comparison of the expected and derived from observations characteristics of absorbers demonstrates that at the observed range of redshifts, $1.7 \leq z \leq 4.5$ we see the self-similar period of structure evolution. During this period the main factors determining the evolution of absorbers such as the pancake expansion, creation and merging, are balanced what leads to relatively slow evolution of the mean properties of absorbers, such as d_{sep} and the DM column density,

q . This slow evolution is supported by slow regular variations of the UV background radiation and the ionization rate, Γ_{12} .

However, at small redshifts, $z \leq 0.5$ the growth of perturbations and merging of absorbers becomes decelerated due to the influence of the Λ -term while expansion and disruption of absorbers remains important. This means that at such redshifts the quiet evolution of absorbers is distorted and we can expect a progressive decrease of linear density of observed absorbers with the hydrogen column density $N_{HI} \geq 10^{12} \text{ cm}^{-2}$. The variations of the population of observed absorbers are also modulated by the poorly known variations of the UV background.

At larger redshifts evolution of DM pancakes is mainly driven by the shape of the initial power spectrum. For the standard CDM-like correlation function (20) we get that the self-similar evolution takes place at redshifts

$$z \leq z_{thr} \sim \sqrt{0.375/q_0} \approx 19 \sqrt{10^{-3}/q_0}, \quad (78)$$

and at $z \geq z_{thr}$ pancakes with $q \sim q_0$ are more abundant.

However, the observational test of these expectations is quite problematic because the observed characteristics of absorbers depend also upon evolution of the background temperature and UV radiation.

5.7 Reheating of the Universe

Recent observations of high redshift quasars with $z \geq 5$ (Djorgovski et al. 2001; Becker et al. 2001; Pentericci et al. 2002; Fan et al. 2002, 2003, 2004) provide clear evidence in favor of the reionization of the Universe at redshifts $z \sim 6$ when the volume averaged fraction of neutral hydrogen is found to be $f_H \geq 10^{-3}$ and the photo ionization rate $\Gamma_\gamma \sim (0.02 - 0.08) \cdot 10^{-12} \text{ s}^{-1}$. These results are consistent with those expected at the end of the reionization epoch which probably takes place at $z \sim 6$.

These results can be compared with expectations of the Zel'dovich approximation (DD04). The potential of this approach is limited since it cannot describe the nonlinear stages of structure formation and, so, it cannot substitute the high resolution numerical simulations. However, it describes quite well many observed and simulated statistical characteristics of the structure such as the redshift distribution of absorbers and evolution of their DM column density. This approach does not depend on the box size, number of points and other limitations of numerical simulations (see discussion in Paper II) and it successfully augments them.

This approach shows (DD04) that at $z \sim 6$ only $\sim 3.5\%$ of the matter is condensed within the high density clouds which can be associated with luminous objects. This value can increase up to $\sim 5 - 6\%$ with more accurate description of the clouds collapse. The same approach also allows one to estimate the mass function of structure elements (DD04) at different redshifts. At $z \sim 6$, the mean DM mass of the clouds is expected to be $\langle M_{cl} \rangle \sim 10^{10} M_\odot$ and majority of clouds have masses between $10^{-3} \langle M_{cl} \rangle$ and $10 \langle M_{cl} \rangle$. The formation of low mass clouds with $M_{cl} \leq 10^6 M_\odot$ is suppressed due to strong correlation of the initial density and velocity fields at scales $\leq l_p \sim 0.03 h^{-1} (q_0/10^{-3}) \text{ Mpc}$ (17). However, the numerous low mass satellites of large central galaxies can be formed in the course of disruption of

massive collapsed clouds at the stage of their compression into thin pancake-like objects (Doroshkevich 1980; Vishniac 1983). The minimal mass of such satellites was estimated in Barkana, Haiman & Ostriker (2001).

This means that the investigation of absorbers observed at high redshifts should be supplemented by the study of properties of dwarf *isolated* galaxies and discrimination between such galaxies and dwarf satellites of more massive galaxies. Such observations seem to be a perspective way to discriminate between models with one and several types of DM particles.

Acknowledgments

This work would not have been possible without the important contribution of M. Rauch and W.L.W. Sargent who provided us with unpublished spectra of five quasars. We are deeply grateful for their permission to use their data. This paper was supported in part by the Polish State Committee for Scientific Research grant Nr. 1-P03D-014-26 and Russian Found of Fundamental Investigations grant Nr. 05-02-16302.

REFERENCES

- Bahcall J.N. et al., 1993, ApJS., 87, 1.
 Bahcall J.N. et al., 1996, ApJ., 457, 19.
 Bardeen J.M., Bond J.R., Kaiser N., Szalay A., 1986, ApJ., 304, 15
 Barkana R., Haiman Z., Ostriker J.P., 2001, ApJ., 558, 482
 Becker R.H. et al. 2001, AJ, 122, 2850
 Becker R.H., Sargent W.L.W., & Raugh M., 2004, ApJ, 613, 61
 Bergeron J., Cristiani S., & Shaver P.A., 1992, A&A, 257, 417
 Bergeron J. & Herbert-Fort S., 2005, "Probing Galaxies through Quasar Absorption lines", IAU Colloquium No.199, eds. Williams P.R., Shu C., & Menard B., astro-ph/0506700
 Bi H., & Davidsen A.F., 1997, ApJ., 479, 523
 Black J.H., 1981, MNRAS, 197, 553
 Boksenberg A., Sargent W.L.W., & Raugh M., 2003, ApJS, submit., astro-ph/0307557
 Carswell R., Shaye J., & Kim T.S., 2002, ApJ, 578, 43
 Cen R., 2003, ApJ, 591, 12
 Ciardi B., Ferrara A., & White S.D.M., 2003, MNRAS, 44, L7
 Cristiani S., D'Odorico V., 2000, AJ, 120, 1648
 Croft R.A.C., Weinberg D.H., Katz N., & Hernquist L., 1998, ApJ., 495, 44
 Croft R.A.C. et al., 2001, ApJ., 557, 67
 Croft R.A.C. et al., 2002, ApJ, 581, 20
 Davé R., Hernquist L., Katz N., Weinberg D.H., 1999, ApJ., 511, 521,
 Demiański M. & Doroshkevich A., 1999, MNRAS., 306, 779, (DD99).
 Demiański M., Doroshkevich A.G., Müller V., & Turchaninov V.I., 2000, MNRAS, 318, 665
 Demiański M., Doroshkevich A.G., & Turchaninov V.I., 2003a, MNRAS, 340, 525, (Paper I)
 Demiański M. & Doroshkevich A.G., 2003b, Apj, 597, 81, (Paper II)
 Demiański M. & Doroshkevich A., 2004a, AA, 422,423, (DD04)
 Demiański M. & Doroshkevich A., 2004b, MNRAS, 354, 183.
 Djorgovski S.G., Castro S., Stern D., Mahabal A.A., 2001, ApJ., 560, L5
 Dodelson S. et al., 2002, ApJ, 572, 140
 Doroshkevich, A.G., 1980, SvA., 24, 152
 Doroshkevich, A.G., Tucker, D.L. Allam S. & Way M., 2004, AA, 418, 7
 Fan X. et al., 2002, AJ, 123, 1247
 Fan X. et al., 2003, AJ, 125, 1649
 Fan X. et al., 2004, AJ, 128, 515
 Frenk C.S., 2002, Philos.Trans.R.Soc. London, 300, 1277
 Gialalisco et al. 2004, ApJ, 600, L103
 Gnedin N.Y. & Hamilton A.J.S., 2002, MNRAS, 334, 107
 Haardt F., Madau P., 1996, ApJ, 461, 20
 Hoekstra H., Yee H., & Gladders M., 2002, ApJ, 577, 595
 Hu E.M., Kim T.S., Cowie L., Songaila A. & Rauch, M., 1995, AJ, 110, 1526
 Hui L., Gnedin N.Y., 1997, MNRAS, 292, 27
 Ikeuchi S., Ostriker J.P, 1986, ApJ., 301, 522.
 Ivanov P., Naselsky P., Novikov I., 1994, Phys.Rev.D, 50, 7173
 Jannuzi B.T. et al. ApJS. 1998, 118, 1
 Kim T.S., Cristiani S., & D'Odorico S., 2002, A&A, 383, 747
 Kim T.S., Carswell R.F., Cristiani S., D'Odorico S. & Giallongo E., 2002, MNRAS, 335, 555
 Kim T.S., Viel M., Haehnelt M., Carswell R.F., Cristiani S., 2004, MNRAS, 347, 355
 Kirkman D., & Tytler D., 1997, ApJ., 484, 672.
 Kogut A., et al., 2003, ApJS, 148, 161
 Komatsu E., et al., 2003, ApJS, 148, 119
 Levshakov S.A., Agafonova I.I., Reimers D., Baade R., 2003, A&A, 404, 449
 Lanzetta K.M., Bowen D.V., Tytler D., & Webb J.K., 1995, ApJ., 442, 538.
 Le Brune V., Bergeron J., & Boisse P., 1996, A&A, 306, 691
 Lu L., Sargent W.L.W., Womble D.S., Takada-Hidai M., 1996, ApJ., 472, 509
 Manning C., 2002, ApJ, 574, 599
 Manning C., 2003a, ApJ, 591, 79
 Manning C., 2003b, ApJ, 595, 19
 Matarrese S. & Mohayaee R., 2002, MNRAS, 329, 37
 McDonald P. et al., 2000, ApJ., 543, 1
 McDonald P. & Miralda-Escude J., 2001, ApJ., 549, L11
 McDonald P. et al., 2001, ApJ., 562, 52
 McDonald P. et al., 2004, astro-ph/0405013, astro-ph/0407377
 McGill C., 1990, MNRAS, 242, 544
 McLin K., Stocke J.T., Weymann R., Penton S.V., Shull M., 2002, ApJ, 574, L115
 Meiksin A., Bryan G., Machacek M., 2001, MNRAS, 327, 296
 Morris S., Weimann R.J., Savage B.D., Gilland R.L., 1993, ApJ, 377, L21
 Morris S., Weimann R.J., Dressler A., McCarthy P.J., 1993, ApJ, 419, 524
 Nusser A., Haehnelt M., 2000, MNRAS, 313, 364
 Oort J.H., 1981, Astr.Astrophys., 94, 359.
 Oort J.H., 1984, Astr.Astrophys., 139, 211.
 Ouchi M., 2005, ApJ, 620, L1
 Peiris H., et al., 2003, ApJS, 148, 213.
 Pentericci L. et al., 2002, AJ, 123, 2151
 Penton S.V., Shull J.M., & Stocke J.T., 2000, ApJ., 544, 150
 Penton S.V., Stocke J.T., & Shull J.M., 2002, ApJ., 565, 720
 Percival W., et al., 2001, MNRAS, 327, 1297
 Polarsky D. & Starobinsky A., 1995, Phys.Lett., B356, 196
 Rauch M., 1998, Ann.Rev.Astr.Astrophys., 36, 267
 Sargent, W.L.W., Young, P.J., Boksenberg, A. & Tytler, D., 1980, ApJ.Suppl, 42, 41
 Schaye J., Theuns T., Leonard A. & Efstathiou G., 1999, MNRAS, 310, 57
 Schaye J. et al., 2000, MNRAS, 318, 817
 Scott J., Bechtold J., Dobrzicki A. & Kulkarni V.P., 2000, ApJS, 130, 67
 Schaye J., 2001, ApJ, 559, 507
 Scott J., Bechtold J., Morita M., Dobrzicki A. & Kulkarni V.P., 2002, ApJ, 571, 665
 Seljak U., McDonald P., Makarov A., 2003, MNRAS, 342, L79
 Seljak U. et al., 2004, astro-ph/0407372

- Shandarin S., Zel'dovich Ya.B., 1989, *Rev.Mod.Phys.*, 61, 185
- Shandarin S. et al., 1995, *Phys.Rev.Let.*, 75, 7
- Simcoe R., Sargent W.L.W., Rauch M., 2002, *ApJ.*, 578, 737
- Simcoe R., Sargent W.L.W., Rauch M., 2004, *ApJ.*, 606, 92
- Spergel D., et al., 2003, *ApJS.*, 148, 175.
- Spergel D., et al., 2006, *astro-ph/0603449*.
- Tegmark M., Hamilton A.J.S., & Xu Y., 2003, *MNRAS*, 335, 887
- Tegmark M., Zaldarriaga M., 2003, *Phys.Rev.D*, 66, 103508
- Tegmark M., et al., 2004, *Phys.Rev.D*, 69j3501
- Telfer R.C., Kriss G.A., Zheng W., Davidsen A.F. & Tytler D., 2002, *ApJ*, 579, 500
- Theuns T., Leonard A., Schaye J., Efstathiou G., 1999, *MNRAS*, 303, L58
- Theuns T., Schaye J., Haehnelt M., 2000, *MNRAS*, 315, 600
- Theuns T., Schaye J., Zaroubi S., Kim T.-S., Tzanavaris P., & Carswell R., 2002a, *ApJ*, 567, L103
- Theuns T., Zaroubi S., Kim T.-S., Tzanavaris P., & Carswell R., 2002b, *MNRAS*, 332, 367
- Turok N., 1996, *ApJ*, 473, L5
- Tytler D., 1995, in Meylan J., ed., *QSO Absorption Lines*, p. 289.
- Verde L., et al., 2002, *MNRAS*, 335, 432
- Verde L., et al., 2003, *ApJS.*, 148, 195.
- Viel M., Matarrese S., Mo J.H., Theuns T., Haehnelt M.G., 2002, *MNRAS*, 329, 848
- Viel M., Haehnelt M.G., Carswell R.F., Kim T.-S., 2004a, *MNRAS*, 349, L33
- Viel M., Haehnelt M.G., Springel V., 2004b, *MNRAS*, 354, 684
- Vishniac E.T., 1983, *ApJ.*, 274, 152
- Wang X., Tegmark M., Jain B., Zaldarriaga M., 2003, *Phys.Rev.D*, 68, 123001
- Weinberg D.H., Burles S., Croft R.A.C., et al., 1998, in "Evolution of Large Scale Structure: From Recombination to Garching", eds. A.J. Banday, R.K. Sheth, L.N. Da Costa, p. 346
- Zaroubi S., Viel M., Busser A., Haehnelt M., Kim T.S., 2005, *MNRAS*, submit. *astro-ph/0509563*
- Zel'dovich Ya.B., 1970, *Astrophysica*, 5, 20
- Zhang Yu., Meiksin A., Anninos P., Norman M.L., 1998, *ApJ.*, 495, 63